Eur. Phys. J. Plus (2025) 140:464
https://doi.org/10.1140/epjp/s13360-025-06315-y

THE EUROPEAN PHYSICAL JOURNAL PLUS

Regular Article

Earthquake waves in a modified Burridge and Knopoff model

Théodule Nkoa Nkomom[1,2,a], **Joseph Brizar Okaly**[2,3,b], **Alain Mvogo**[2,c]

[1] Department of Physics, Higher Teachers Training College of Bertoua, University of Bertoua, Bertoua, Cameroon
[2] Department of Physics, Faculty of Science, University of Yaounde I, Yaounde, Cameroon
[3] Department of Physics, Government High School Minkama, Ministry of Secondary Education, Obala, Cameroon

Received: 13 November 2024 / Accepted: 10 April 2025

Abstract The propagation of nonlinear waves in a mass-spring system modelled by a modified Burridge and Knopoff model for earthquakes is studied. The spatio-temporal dynamics of the system is found by taking into account the hydrodynamic coupling damping forces, the stiffness of the elasticity of the rock material in a nonlinear form, and the empirical friction forces experimentally approved. The blocks are placed on a downward slope with an angle θ with respect to the horizontal line. The theoretical framework for the analysis shows that the system can be reduced into two components: an oscillating part and a non-oscillating part. While the oscillating part is a nonlinear earthquake wave equation describing the behaviour of the earthquake waves propagating in the Earth crust, the non-oscillating part is a landslide equation describing the displacement of the ground during the shock. In the semi-discrete approximation, the nonlinear earthquake wave equation is shown to be governed by a dissipative bright-like soliton solution of the complex Ginzburg–Landau (CGL) equation, while the ground displacement equation is reduced to the residual displacement of the blocks observed after the ground shaking. The relationship between landslide and floor velocity is found, showing that whether there is a slope or not, any earthquake-induced ground displacement whose importance depends on the duration of the ground shaking and the angle slope. In the linear limits, the system is found governed by a dissipative plane wave solution of the complex linear Schrodinger (CLS) equation. Also, we found that the amplitude and frequency vibration of the earthquake wave decreases due to friction (as well as to stiffness of rock material), while the inverse effect is observed on the propagation area.

1 Introduction

Nowadays, the prediction of the earthquakes and the prevention of related damages, such as human life lost and destruction of movable and immovable property, is the great challenge in modern nonlinear physics. An earthquake is a sudden oscillation of the Earth crust due to the synergistic movements with respect to each other of the individual elements of a geological environment at different scales, occurring within the seismic focus at the edge of emerging active faults [1]. The propagation of earthquake waves along the Earth crust arrives naturally and occurs suddenly at places in the world where a fault breaks, causing a sudden stress relief on the Earth crust exceeding a certain critical value [2, 3].

The size of an earthquake can differ, and sometimes, it is said that weak earthquakes are not felt either, but the most violent can cause major damage, such as the destruction of entire cities. Strong earthquakes are typical examples of disasters, as they cause significant loss of life and economic damage. There is a relationship between the magnitude of the earthquake, the dimensions of the fault that ruptured, and the offset between the two blocks separated by the fault. The greater the rupture surface at basement level, the faster it moves and the more powerful the earthquake. Showing that, the strength of an earthquake depends not only on its type or size experienced over a period of time but also on the geology of the city. For instance, the *Valdivia* earthquake which occurred in Chile on May 22, 1960, which attends 9.5 on the Richter scale [4], is until now the largest earthquake ever recorded by a seismic network. The ground shaking was followed by a devastating tsunami, the destructive effects of which were felt throughout the Pacific. It was a mega-thrust event, which will have left more than 5000 dead or missing in Chile, Japan, and Hawaii [5–7].

In addition, a relevant theoretical mathematical model by Burridge and Knopoff (BK) [8] was introduced 50 years ago. The model, which can be seen as evidence of critical self-organization, consists of rock blocks coupled to each other by spring interactions and to a driver plate by another spring interaction. The rock materials are discrete; they are made up of grains, crystals, or blocks

Joseph Brizar Okaly and Alain Mvogo have contributed equally to this work.

[a] e-mail: theodulenkoa@yahoo.fr
[b] e-mail: okalyjoseph@yahoo.fr (corresponding author)
[c] e-mail: mvogal_2009@yahoo.fr

Published online: 30 May 2025

of different sizes separated from each other by cracks of all possible sizes. The blocks are placed on a rough surface, moving to the right. Friction between the two tectonic plates consists of the driver plate and the moving surface (see Fig. 1). The numerical simulations of the model have been compared to laboratory experiments, and the results were completely disconnected.

In the last couple of years, based on the BK model, numerous theoretical mechanical models have been set out in an attempt to reduce the gap between laboratory experiments and simulation; and to explain the behaviour of rock material and other observations of successive spatio-temporal events arriving during and after an earthquake [3, 9–12]. Although the observations of natural earthquakes were similar to the results of numeric simulations of the models [8, 11], the gap between the laboratory experiments and simulations of the model still exists. Also, these studies have left out the landslide by neglected their impacts on the ground shaking. Since the naturals earthquakes generally induced landslide with its devastating effects, in this paper, a detailed study of the ground displacement due to the propagation of earthquake waves is done.

To reduce the ditch between laboratory experiments, theory, and natural observations, simplified models in which the motion of the blocks is induced by the strengths due to friction were implemented. The works focused on the single or two spring-block model associated with the nonlinear elastic properties of rock material and the type of friction.

Along the same lines, in this paper, we extend the BK model by introducing new external interactions in order to take into account something long ignored by many researchers on the BK model but nevertheless very present as a consequence of most earthquakes: the landslides. Although the hydrodynamics damping friction forces and nonlinear stiffness of the elasticity of rocks with velocity-dependent friction on the exponential type have been taken into account in recent works by us [13, 14], in the present paper, we consider these interactions and add new ones, such as the pulling forces by the driver plate. Instead of the exponential friction used previously, we use experimental empirical frictions [1]. We also consider that the blocks are placed on a tilted slope with an angle θ compared to the horizontal line.

For this purpose, using the above-mentioned modified BK model, we show that the nonlinear properties of the mass-spring system are completely described by two components: an oscillating part governed by the bright-like soliton of the CGL (as well as the plane wave solution of the CLS) equation, which represents the earthquake waves moving along the Earth crust; and a non-oscillating part related to the boundary conditions, which represent the residual displacement of the blocks observed after the earthquakes waves propagation. Since landslides cause more than 50% of the damage attributed to earthquakes, particular attention is paid to the residual displacement, which is the distance travelled by the ground during the propagation of earthquake waves. Numerically, relevant results are obtained, showing qualitatively the good agreement between the present model, experiments, and natural observations. Therefore, the model under study is suitable to describe many phenomena that take place during an earthquake.

The rest of the paper is outlined as follows: In Sec. 2, the Lagrangian model and equation of motion are presented. A detailed analysis of the non-oscillating part is also done. In Sec. 3, using the multiple scale expansion in the semi-discrete approximation, the wave equation of the oscillating part of the system is reduced to a the CGL equation with the bright-like soliton (as well to the CLS equation with the plane wave) solution. In Sec. 4, we present our main results and discussions. In Sec. 5, the paper concludes.

2 Model and equations of motion

We strongly rely on the Burridge–Knopoff (BK) model of earthquakes, introduced 50 years ago. The model consists of two tectonic plates consisting of N identical blocks of rock materials connected through N springs in series with a normal length b_0 and a spring constant K representing the stiffness coefficients of the elastically interacting. The blocks are also connected to a driving plate with a pulling spring of strength J. The model considers the earthquakes caused by the friction between the two tectonic plates. Although the model showed relevant results, such as similarity to real earthquakes, it is not always sufficient for artificial earthquakes.

Thus, to reduce the gap with experiments, the model was extended to well describe the elastic properties of rock material and the friction between the two tectonic plates.

While the leftmost block is connected to a fixed wall, all the blocks are initially ($t = 0$) placed, in the interval of a, on a rough surface moving to the right with a constant velocity u. The blocks, which are subject to external forces, accumulate energy in springs due to small vibrations of the blocks from their equilibrium positions. The velocity-dependent friction of empirical type experimentally approved, and hydrodynamic damping forces are also adopted (see Fig. 1 and Fig. 2).

It is obvious from Fig. 1 that

$$T = \frac{1}{2}m\dot{x}_n^2, \quad U = \frac{1}{2}K(x_n - x_{n+1})^2, \tag{1}$$

where T is the kinetic energy, and U is the potential energy, with the equal mass m of the rock blocks, and K is the coupling springs strength. The letters x_n denote the coordinates of the blocks, while n defines the position of the blocks. The x-axis is directed along the fault. So, the Lagrange equations of motion of the model have the following form,

$$\frac{d}{dt}\left(\frac{\partial T}{\partial \dot{x}_n}\right) + \frac{\partial U}{\partial x_n} = \sum_i F_n^i, \tag{2}$$

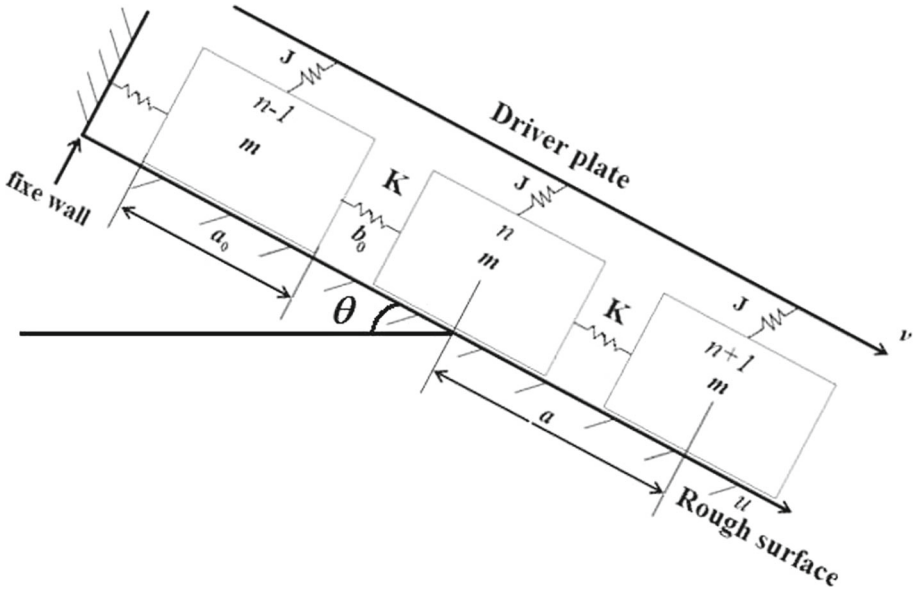

Fig. 1 Schematic representation of the mass-spring system of the model. The system is assumed to be spatially homogeneous, with blocks of a cubic form with equal dimension a_0 and mass m. Each block is connected to adjacent ones through springs of strength K. Each block is also connected to the upper surface with another spring (the pulling spring) of strength J. The blocks are initially placed on a tilted floor with a rough surface moving to the right with a constant velocity u. The leftmost block is connected to a fixed wall. The equilibrium spacing between two neighbouring blocks is a associated with the length of the relaxed spring b_0

where $\sum_i F_n^i$ denotes all the external forces acting on the block with respect to the block position n. In their pioneering work, Burridge*et al.* [8] considered external forces only the action of the driver plate on the blocks, which represents the "pulling" force for the neighbouring spring. The force is in the form of

$$F_n^{(2)}(x_n) = -J(x_n - vt), \tag{3}$$

with J being the stiffness of the elasticity of rocks.

The BK model represented by Eq. (2) has shown important limits as the ditch between laboratory experiments and numerical simulations. Thus, to reduce the ditch between experiments and theory, in the present, we introduce some friction forces experimentally observed, such as the hydrodynamic friction forces $F_n^{(1)}$ [13–16], and the friction forces by Leonardo da Vinci [1] $F_n^{(3)}$. The importance of these forces is not much to show. For instance, due to the interactions between particles of the system, which can be electrostatic, Van der Waals, or other types [17], the motion of one particle strongly depends on the motions of the other particles of the system. Thus, hydrodynamic friction forces are of greater importance in the nonlinear sciences. Also, in spite of the complexity of the friction process, the above law of friction forces introduced by Leonardo da Vinci [1], which represents the friction forces at the lower boundary of the blocks, is commonly used in engineering applications. We have,

$$F_n^{(1)}(\dot{x}_n) = \gamma^{hy}(\dot{x}_{n+1} - 2\dot{x}_n + \dot{x}_{n-1}), \quad F_n^{(3)}(\dot{x}_n) = \mu G \sin\theta, \tag{4}$$

where

$$\mu = b + r\big[1 + \beta(u - \dot{x}_n)\big]^{-1}, \quad \text{with} \quad r = p - b. \tag{5}$$

The parameter u is the constant velocity with which the floor on which the rock blocks are placed is moving. The parameter G is the load of blocks on a moving main plate, which practically coincides with the weight of blocks $G = mg$ (m is the mass of the block, and g is gravity acceleration), with μ being the experimental empirical coefficient of friction depending on the relative velocity $V = u - \dot{x}_n$ and θ the angle between the horizontal line and the surface on which the blocks are placed. γ^{hy} being the elastic hydrodynamic damping coupling constant. The friction is characterized by p the coefficient of friction at rest ($V \longrightarrow 0$), b the steady-state limiting value of the friction coefficient at high velocities ($V \longrightarrow \infty$), and β the dimensionless empirical constant with a dimension of inverse speed. The velocity $V^{(1)} = \beta u$ is the speed of the flank surface of the fault, while the velocity $V^{(2)} = \frac{1}{\beta}$ is the characteristic relative velocity.

To mimic experimental observation, the nonlinear elasticity of rock material should also be taken into account. It is well known by geologists that J does not have the same value for large contractions and dilations. Indeed, stiffness decreases when going from contraction to dilation. When it achieves a certain value, which is seen as a critical value, the rock crashes. The description of such behaviour is easily done by adding cubic and quadratic terms to the stiffness forces, as done in Eq. (6). Meanwhile, the nonlinear stiffness used in the present paper has a physical sense.

This is achieved by considering the stiffness of the elasticity of rock material in the nonlinear form instead of the linear commonly used [2]. So, in the following, the stiffness of the elasticity of rock is assumed in the form

$$F_n^{(4)}(x_n) = -J\left[x_n + \epsilon\left(\frac{1}{b_0}x_n^2 + \frac{1}{2b_0^2}x_n^3\right)\right], \tag{6}$$

with b_0 being the length of relaxed spring and $\epsilon \ll 1$ a small real number measuring the nonlinear elasticity of the rock material.

The equation of motion is obtained by introducing Eqs. (1), (3), (4), and (6) in Eq. (2),

$$\begin{aligned}\ddot{x}_n =&\frac{K}{m}\Big(x_{n+1}-2x_n+x_{n-1}\Big)-\frac{J}{m}(x_n-vt)-\frac{J}{m}\left[x_n+\epsilon\left(\frac{x_n^2}{b_0}+\frac{x_n^3}{2b_0^2}\right)\right]\\&+\frac{\gamma^{hy}}{m}\Big(\dot{x}_{n+1}-2\dot{x}_n+\dot{x}_{n-1}\Big)+\Big(b+r\big[1+\beta(u-\dot{x}_n)\big]^{-1}\Big)g\sin\theta.\end{aligned} \tag{7}$$

Equation (7) is the equation that describes the motion of a block rock during an earthquake in the modified BK model by considering the friction at the lower boundary of the blocks, hydrodynamic friction, and nonlinear elasticity of rock material.

When investigating the dynamics of large intra-continental and suboceanic faults, Khain and Lomeeze [18] clearly indicate that the average rate of the velocity of relative motion of the edges of the faults does not exceed 3.10^{-9} m/s. Although the study was done over large time intervals and the data were strongly averaged. It describes the slow creep of the edges of the faults [19]. Indeed, at the scale of earthquake duration, the relative speed of the fault edges V can reach large values similar to the values of the velocity of oscillations of seismogenic blocks. For instance, during the earthquake in Parkfield (California, June 28, 1966) [20], the speed of soil particles reached 0.76 m/s. From the above-mentioned works, it clearly appears that the values of the relative velocity $V = u - \dot{x}_n$ are naturally small as compared to the unit. Then, without losing sufficient accuracy for practice, we expand the velocity-dependent friction forces in the Taylor series, and we consider only terms < 2, such that

$$\Big[1+\beta(u-\dot{x}_n)\Big]^{-1}\approx 1-\beta(u-\dot{x}_n) \tag{8}$$

Inserting Eq. (8) in Eq. (7) yields,

$$\begin{aligned}\ddot{x}_n =&\frac{K}{m}\Big(x_{n+1}-2x_n+x_{n-1}\Big)-\frac{J}{m}(x_n-vt)-\frac{J}{m}\left[x_n+\epsilon\left(\frac{x_n^2}{b_0}+\frac{x_n^3}{2b_0^2}\right)\right]+\frac{\gamma^{hy}}{m}\Big(\dot{x}_{n+1}-2\dot{x}_n+\dot{x}_{n-1}\Big)\\&+(\beta rg\sin\theta)\dot{x}_n+(p-\beta ru)g\sin\theta.\end{aligned} \tag{9}$$

Let us introduce a dimensionless time,

$$t=\omega_p t,\quad \omega_p^2=\frac{J}{m}. \tag{10}$$

Thus, Eq. (9) becomes,

$$\begin{aligned}\ddot{x}_n =&K_1\Big(x_{n+1}-2x+x_{n-1}\Big)-(x-v_1t)-\left[x_n+\epsilon\left(\frac{x_n^2}{b_0}+\frac{x_n^3}{2b_0^2}\right)\right]+\gamma_1^{hy}\Big(\dot{x}_{n+1}-2\dot{x}_n+\dot{x}_{n-1}\Big)\\&+\gamma_1\dot{x}_n+\Big(p_1-\beta r_1u\Big)g\sin\theta,\end{aligned} \tag{11}$$

where

$$K_1=\frac{K}{m\omega_p^2},\quad \gamma_1^{hy}=\frac{\gamma^{hy}}{m\omega_p},\quad \gamma_1=\gamma_2\sin\theta,\quad \gamma_2=\frac{\beta rg}{\omega_p},\quad v_1=\frac{v}{\omega_p},\quad p_1=\frac{p}{\omega_p^2},\quad r_1=\frac{r}{\omega_p^2}.$$

The dimensionless constants K_1, γ_1^{hy}, g_1, v_1, and γ_1, and γ_2 are the stiffness of the coupling spring, hydrodynamic elastic coupling, gravity, pulling speed, and the "static friction" constants, respectively.

The dimensionless speed of the driver plate can be rewritten as $v_1=\frac{\omega_p^{-1}}{v^{-1}}=\frac{t_s}{t_l}$. Such that the parameters t_s and t_l are the slipping time (the inverse dimensionless constant) and the loading time (the inverse speed of the driver), respectively. The loading time represents the necessary time for which the pulling spring stretches enough to overcome the static friction.

The function v_1t is the distance travelled by the plate with respect to the duration t of the earthquake. However, in the framework of the earthquakes, the ground shaking is limited in time. Usually, an earthquake lasts a few seconds, but the strongest can last a few minutes. For example, the most powerful and devastating earthquake occurred in Chile in the region of *Valdivia* in 1960, when the ground was shaken for about 5 min (300 s). Moreover, generally, in earthquake faults, the slipping time is of the order of a second, and the loading time is of the order of tens or hundreds of years, allowing the velocity of the fault edge to be of the order of a millimetre by years ($\sim 10^{-11}$ m.s^{-1}). Optimistic studies locate it around $\sim 10^{-9}$ m.s^{-1} [18, 21]. Therefore, v_1t is relatively a constant. Thus, for our purpose, in the following, this distance is assumed to be expressed in time units [22], yielding the equation shown below,

$$\begin{aligned}\ddot{x}_n =&K_1\Big(x_{n+1}-2x+x_{n-1}\Big)-2\Big[x_n+\epsilon\Big(\alpha_2x_n^2+\alpha_3x_n^3\Big)\Big]+\gamma_1^{hy}\Big(\dot{x}_{n+1}-2\dot{x}_n+\dot{x}_{n-1}\Big)+\gamma_1\dot{x}_n\\&+\Big[v'+\Big(p_1-\beta r_1u\Big)g\sin\theta\Big],\end{aligned} \tag{12}$$

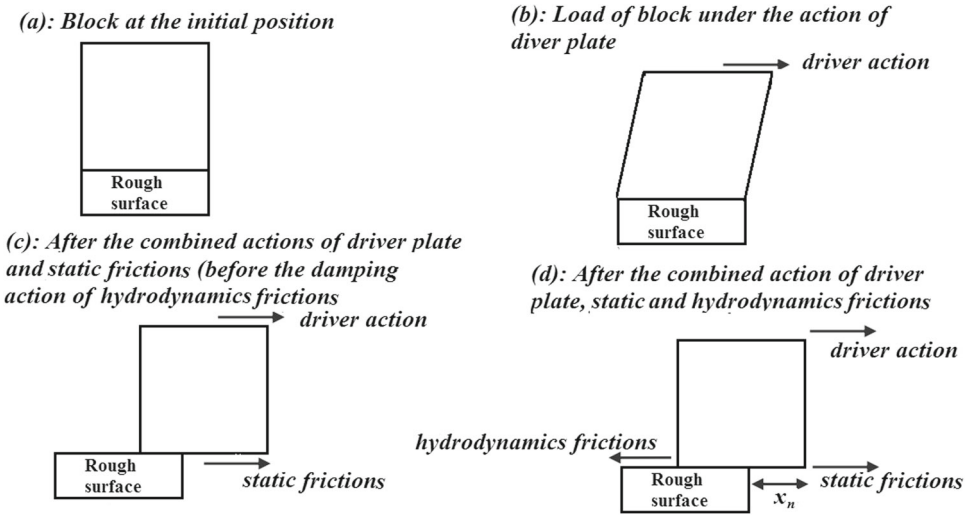

Fig. 2 Schematic representation showing the effect of driver plate, friction, and hydrodynamics interactions on the Earth crust

where $\alpha_3 = \alpha_2^2$, $\alpha_2 = \frac{1}{2b_0}$, and $v' = v_1 t$.

Equation (12) is a dimensionless nonlinear differential equation governing the dynamics of a nonlinear seismic wave propagating in a mass-spring system, taking into account the velocity-dependent friction and hydrodynamic damping forces.

In the next sections, the dimensionless parameters of the system are $\gamma_1^{hy} = 0.1$, $\gamma_2 = 0.01$, $K_1 = 1$, $\epsilon = 0.01$, $\varepsilon = 0.1$, $b_0 = 1$, a=0.0003 g=9.73, $\beta = 1$, $v' = 0.1$, $p_1 = 0.1$, $r_1 = 1$.

The variable x_n has two components, a non-oscillating part and an oscillating part. The oscillating part, which depends on space and time, represents the slip of the n^{th} block from its adjacent position on the driving plate, and the non-oscillating part is related to the boundary condition [13].

Accordingly, the solution x_n of Eq. (12) is assumed to be of the form

$$x_n(t) = v_n(t) + \rho, \tag{13}$$

where

$$\rho = \rho_0 + \rho', \quad \text{with} \quad \rho_0 = \frac{1}{2}v', \quad \rho' = \frac{1}{2}\Big(p_1 - \beta r_1 u\Big) g \sin\theta.$$

The oscillating part v_n represents the nonlinear earthquake waves propagating in the media. Although the non-oscillating part ρ is related to the boundary condition [13], it is known as the landslide, which represents here the residual displacement of the blocks observed after the shocks [23]. The residual displacement content is divided into two terms. The first term, ρ_0, is the residual displacement due to the driver plate, while the second term, ρ', represents the residual displacement due to the slope.

Equation (13) clearly shows that any earthquake induces a landslide, whose importance depends strongly on the duration of the shock. That is, whether there is a slope or not, an earthquake can cause a landslide, which is an increasing function of the duration of the ground shaking. It means that the longer the earthquake lasts, the bigger the landslide. In the absence of a slope, sliding depends solely on the speed of the plate. But in the presence of a slope, it depends not only on the speed of the plate but also on the angle of the slope. The slope is just an amplifying factor of the landslide and not a creating factor. In Fig. 3, we depict the evolution of the residual displacement in terms of the slope angle θ (see Fig. 3a) and in terms of the floor velocity u (see Fig. 3b), respectively. It is noticed that the residual displacement increases with θ and decreases with u. The evolution of the critical velocity u_{cr} in terms of the slope angle θ is also depicted (see Fig. 3c), showing its decreasing with θ up to a limiting value $u_{cr} = u_0 = 1.103$.

From Eq. (13), it is noticed that the residual displacement is the function of the speed of both the driver plate v_1 and floor u and the friction characteristics p_1, r_1, and β. The residual displacement presents opposite behaviours, depending on whether v_1 or u evolve. It increases with v_1 and decreases with u. Moreover, it is also observed that the residual displacement increases with time.

Generally, earthquakes trigger land movements. Indeed, if the earthquake occurs on difficult, swampy or marshy ground or on a sloping or mountainside, the ground shaking due to the earthquake triggered a translation displacement of rock block material. This displacement of rocks is most often manifested by the formation of ice jams on watercourses, debris flows following the input of materials into watercourses, floods, rock falls, landslides, mudslides, avalanches, folds, faults, overlapping, haulages, and other damage to the crust with disastrous consequences for human life and economic activities.

Usually considered earthquake-induced effects, the landslides triggered by earthquakes are widely considered the primary cause of loss of life, damage to structures, and injuries observed during and after the propagation of earthquake waves. They are responsible for a large part of the damage associated with earthquakes, such as spectacular structural collapses [24, 25]. The landslides induced by an earthquake are generally shallow. However, the volume of displaced ground can sometimes reach a million m^3 and cover

a long distance ($\sim$ 50 km) from the epicentre at high speed ($\sim$ 280 km/h) and cause more than a third of the victims and other associated damage [26–29].

Although most earthquakes are mild and therefore not felt at all by humans, those of a certain magnitude (greater than five on the Richter scale) usually cause landslides. The intensity and extent of these landslides depend largely on the magnitude of the earthquake and the type of soil. The greater the magnitude of an earthquake, the greater the distance travelled by ground from the epicentre [30]. Some earthquakes can even reactivate old ground movements, as was the case during the earthquakes of January 12, 2010, in Haiti, November 14, 2016, in New Zealand, and March 11, 2011, in eastern Japan. It is widely recognized that the consequences of huge earthquakes and resulting landslides can affect the gravity of the Earth, modify its rotation, and therefore the length of day [31–33]. Thus, a detailed analysis of the translation displacement of blocks is of great practical and scientific interest.

However, the real landslide observed during a natural earthquake can be more or less than the one predicted in this paper, due to the type of soil and other geophysical parameters. Indeed, in the following, we restricted ourselves to the landslide caused by the propagation of earthquake waves through the modified BK model proposed in this paper. Other sources of landslides, such as the natural instability of the ground, the type of soil, or the activation of older sources, have been omitted.

Moreover, as experimentally expected, the residual displacement (see Eq. (13)) must increase with the angle of slope θ. This can be observed if and only if the floor velocity u is selected in a finite interval, namely

$$0 \leq u \leq u_0, \quad \text{with} \quad u_0 = \frac{p_1}{\beta r_1}. \tag{14}$$

From Eq. (13), it resulting an optimal velocity,

$$u_{cr} = u_0 + u', \quad u' = \left(\frac{v'}{\beta r_1 g}\right)\left(\frac{1}{\sin\theta}\right), \tag{15}$$

for which the residual displacement vanishes. Meanwhile, for the floor moving at the optimal velocity u_{cr}, the blocks return to their initial positions after the earthquake. Indeed, for $u = u_{cr}$, the residual displacement vanishes, and for $u < u_{cr}$, the residual displacement can be observed. Moreover, from Eqs. (14) and (15), one has $u \leq u_0 \leq u_{cr}$, showing that theoretically, any propagation of nonlinear earthquake waves can induce more or less significant ground displacement [34] $\rho \geq \rho_0$, with ρ_0 being the minimum displacement corresponding to the maximum floor speed u_0 (see Eq. (13)).

Thus, inserting Eq. (13) in Eq. (12) and after removing the secular terms, one has

$$\ddot{v}_n = K_1\left(v_{n+1} - 2v_n + v_{n-1}\right) - 2\left[v_n + \epsilon\left(\alpha_2 v_n^2 + \alpha_3 v_n^3\right)\right] + \gamma_1^{hy}\left(\dot{v}_{n+1} - 2\dot{v}_n + \dot{v}_{n-1}\right) + \gamma_1 \dot{v}_n. \tag{16}$$

Equation (16) represents the nonlinear equation describing the propagation of the earthquake wave along the Earth crust.

The function ρ represents the translation displacement of the blocks due to the earthquake. It depends only on the parameters of the system, friction characteristics, gravity, pulling, and floor velocities; showing that the landslide is related to the characteristics of the fault and the type of soil on which the earthquake occurs. It is also noted that the displacement does not vanish, showing that any propagation of an earthquake wave is accompanied by a ground displacement, which could create folds, faults, overlapping, haulages, and other damage to the crust with disastrous consequences for human life.

The displacement increased when the slope angle evolved. The steeper the slope, the greater the displacement. Although the landslide due to the earthquake increases with respect to the slope angle, the influences of other geophysical factors (such as climate or type of soil) are very important; they make the ground very unstable, which constitutes a real risk for neighbouring living populations.

3 Mathematical analysis and solution of the equation of motion of the amplitude

In this section, the importance of the parameter ϵ (see Eq. (6)) is investigated. Mathematically, the value of ϵ defines the nonlinear character of the system. The case $\epsilon = 0$ corresponds to a linear system, while $\epsilon \neq 0$ is related to the nonlinear system. However, in geology, the stiffness of rock material is not constant; it increases monotonously when rock material goes from dilatation to contraction, and then, when achieving a certain critical value, the rock crashes [35]. Thus, from Eq. (6), it is seen that ϵ measures the stiffness of rock material. Accordingly, one can observe three theoretical situations. The first case corresponds to $\epsilon = 0$, where the rock material is in the dilation state. In this case, nonlinear effects vanished; only linear properties can be observed. The second case corresponds to $\epsilon = 1$, in which the rock material is in the contraction state. In this case, the nonlinear effects are very important; the linear effects are very weak and sometimes insistent. The last and the third case correspond to $0 < \epsilon < 1$. In this case, the rock material is none in the dilatation case and none in the contraction case. One can observe the superposition of both effects, linear and nonlinear. This situation is the most commonly found in nature.

3.1 Nonlinear solution of the equation of motion

In this part, the nonlinear case for which $0 < \epsilon < 1$ is investigated. As in Ref. [36], an exact and numerical approximations solution of Eq. (16) with the related graphical representation can be found using the computational mathematical software MATHEMATICA.

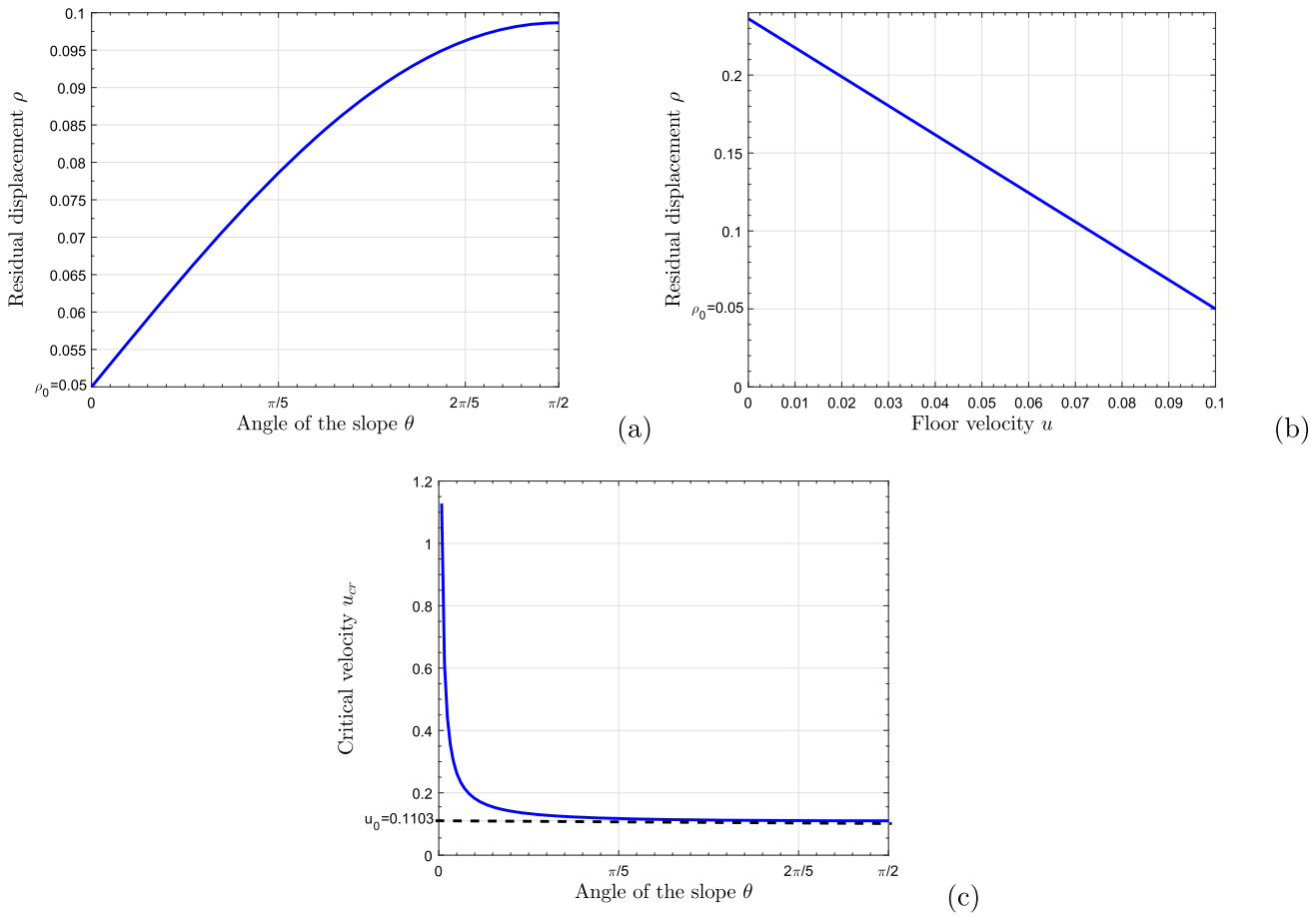

Fig. 3 Evolution of some system parameters at t=1. Panel (**a**) and panel (**c**) present the evolution of the residual displacement and critical velocity in terms of the slope angle, while panel (**b**) presents the evolution of the residual displacement in terms of the floor velocity

However, one of the aim of this work is to find the evolution of the envelope soliton, which represents the amplitude of the earthquakes waves. For this, the multiple scale expansion method in the semi-discrete approximation appears to be the appropriate mathematical tool [37–39], since the spring interactions between adjacent rock blocks are weak. The technique is a powerful perturbation technique for which the carrier waves are kept discrete while their amplitude is treated in the continuum limit. For this purpose, in the following, the amplitude of the wave is assumed to be large enough to be anharmonic and still small compared to the amplitude of the rock blocks. Thus, in the small-amplitude oscillation, a special collective motion of rock blocks is assumed. Therefore, the study of the modulation of the wave is done by setting the soliton solution of Eq. (16) in the form

$$v_n = \varepsilon\Big[F_{1,n}\,\mathrm{e}^{\,\mathrm{i}\theta_n} + F^*_{1,n}\,\mathrm{e}^{\,-\mathrm{i}\theta_n}\Big] + \varepsilon^2\Big[F_{0,n} + \Big(F_{n,2}\,\mathrm{e}^{\,2\mathrm{i}\theta_n} + F^*_{2,n}\,\mathrm{e}^{\,-2\mathrm{i}\theta_n}\Big)\Big], \tag{17}$$

where ε is a small real number ($\varepsilon \ll 1$), $\theta_n = qan - \omega t$, the phase of the soliton with the complex angular frequency of the rock blocks vibrations ω. a is the equilibrium distance of neighbouring rock blocks, and q is the associated wavenumber. The nonlinear terms present in Eq. (16) allow us to predict through frequency superposition that the first harmonics of the wave will contain terms without any exponential dependence as well as terms in $e^{\pm 2\mathrm{i}\theta_n}$. The amplitudes $F_{1,n}$, $F_{0,n}$, and $F_{2,n}$ are considered to change slowly in space and time. Thus, the functions F_0 and F_2 are found as

$$F_0 = -2\epsilon\alpha_2|F_1|^2, \quad F_2 = (BC + iDC)F_1^2, \tag{18}$$

where

$$B = (4\omega_r - \varsigma) - 2\chi(2\chi - \gamma'), \quad C = \frac{2(\epsilon\alpha_2)}{B^2 + D^2}, \quad D = \omega_r\big[4\chi + 2(2\chi - \gamma')\big], \quad \gamma' = \gamma_1 - 4\gamma_1^{hy}\sin^2(qa),$$
$$\omega = \omega_r + \mathrm{i}\,\omega_i, \quad \omega_r = \sqrt{\omega_0^2 - \chi^2}, \quad \omega_i = -\chi, \quad \varsigma = 2 + 4K_1\sin^2(qa), \quad \omega_0^2 = 2 + 4K_1\sin^2\Big(\frac{qa}{2}\Big)$$
$$\chi = \frac{1}{2}\gamma, \quad \gamma = \gamma_1 - 4\gamma_1^{hy}\sin^2\Big(\frac{qa}{2}\Big).$$

The real and imaginary parts of the parameters under consideration are identified by the subscripts r and i, respectively. Then, in the co-moving reference frame at the velocity v_g, by setting $x = \varepsilon(na - v_g t)$, with the rescaled time $\tau = \varepsilon^2 t$. Equation (16) is reduced to [37]

$$i\frac{\partial F_1}{\partial \tau} + (P_r + \mathrm{i}\, P_i)\frac{\partial^2 F_1}{\partial x^2} + (Q_r + \mathrm{i}\, Q_i)|F_1|^2 F_1 = 0, \tag{19}$$

where

$$P_r = \frac{1}{2\omega_r}\left[a^2\left(K_1 - \chi\gamma_1^{hy}\right)\cos(qa) - (v_{g,r}^2 - v_{g,i}^2)\right], \quad P_i = -\left[\frac{1}{2}a^2\gamma_1^{hy}\cos(qa) + \frac{v_{g,r}v_{g,i}}{\omega_r}\right],$$
$$Q_r = -\frac{2\epsilon\alpha_2}{\omega_r}\left[-2\epsilon\alpha_2 + \frac{3}{2}\alpha_2 + BC\right], \quad Q_i = -\frac{2\epsilon\alpha_2}{\omega_r}CD,$$
$$v_{g,r} = \frac{a}{\omega_r}(K_1 - \chi\gamma_1^{hy})\sin(qa), \quad v_{g,i} = -a\gamma_1^{hy}\sin(qa).$$

From Eq. (19), we define a new parameter $c_2 = P_r Q_i - P_i Q_r$. Conte and Musette [40] have shown that the value of c_2 determines the type of the nonlinear equation. If $c_2 = 0$, we are dealing with a complex nonlinear Schrodinger equation (CNLS), i.e. a nonlinear Schrodinger equation (NLS) with complex coefficients. On the other hand, if $c_2 \neq 0$, we are dealing with a complex Ginzburg–Landau (CGL) equation. In this work, this parameter was plotted as a function of the wave vector qa (see Fig. 4c), and as a function of the stiffness of the rock material ϵ (see Fig. 4 d). The lines in both figures show that $c_2 \neq 0$, showing that the equation of interest is a CGL equation with the loss/gain term $\gamma = 0$.

Thus, Eq. (19) is the CGL equation governing the propagation in the Earth crust of envelope waves of nonlinear earthquake waves. The slowly varying function $F_1(x, \tau)$ describes the evolution of the normalized envelope wave with the new scaled space and time coordinates, $x = \varepsilon(z - |v_g|t)$ and $\tau = \varepsilon^2 t$. The coefficients $P = (P_r + \mathrm{i}\, P_i)$, $Q = (Q_r + \mathrm{i}\, Q_i)$, and $v_g = (v_{g,r} + \mathrm{i}\, v_{g,i})$ may be the dispersion, nonlinearity, and group velocity of the wave, respectively. The parameter ω_0 is the angular frequency of the wave in the absence of frictions. In fact, P_r is the wave dispersion, and Q_r is the effective nonlinearity describing how the wave frequency is amplitude modulated. The occurrence of solitons in the system is due to the composite interplay between both parameters. While P_i is related to the relative growth rate of perturbations, Q_i is the cubic nonlinearity damping term measuring the saturation of the unstable wave.

Introduced 70 years ago by Ginzburg and Landau [41, 42], the CGL is one of the most powerful equations used in modern nonlinear physics. In the last couple of years, the CGL equation and their modified versions were successfully used to describe qualitatively and quantitatively nonlinear phenomena in the nonlinear sciences [15, 43, 44]. The CGL equation is difficult to solve; its solutions are always stationary and depend on the mathematical technique used and the problems of interest. Consequently, these solutions, which are non-conservative, do not exist as families of solutions. Although the solutions of CGL equations are dissipative solutions and exist for a limited lifetime before eventually vanishing [43], they describe with good accuracy dissipative nonlinear systems, which usually involve gain or loss of matter or energy [45, 46].

Equation (19) is nonintegrable since it exhibits chaotic behaviour [40]. Only some particular form of solutions can be found related to the problem of interest. The soliton solution of Eq. (19) is given by [16, 47]

$$F_1(x,\tau) = f(\tau)\,\mathrm{sech}\,[L(\tau)(x - x_0)]^{1+\mathrm{i}\,\sigma}\,\mathrm{e}^{\,\mathrm{i}\,\varpi(\tau-\tau_0)}, \tag{20}$$

where

$$f(\tau) = f_0\,\mathrm{e}^{-\gamma_0(\tau-\tau_0)}, \quad f_0 = u_e\sqrt{\frac{1-2\mu}{2P_{2,r}Q_r}}, \quad L(\tau) = L_0\,\mathrm{e}^{-\gamma_0(\tau-\tau_0)}, \quad L_0 = \sqrt{\frac{Q_r}{2P_{2,r}}}f_0,$$
$$\gamma_0 = P_{1,i}L_0^2, \quad \varpi_0 = P_{1,r}L_0^2, \quad \sigma_\pm = \frac{-c_1 \pm \sqrt{\Delta}}{2c_2},$$

with

$$P_{2,r} = P_r - \frac{1}{2}\sigma[3P_i + \sigma P_r], \quad P_{1,r} = P_r - \sigma[2P_i + \sigma P_r], \quad P_{1,i} = P_i + \sigma[2P_r - \sigma P_i],$$
$$c_2 = P_r Q_i - P_i Q_r, \quad c_1 = P_r Q_r + P_i Q_i, \quad c_0 = -2c_2, \quad \Delta = 9c_1^2 + 8c_2^2,$$
$$0 \le \mu < 0.5, \quad P_{2,r}Q_r > 0, \quad c_2 \neq 0.$$

In Fig. 4, we present the evolution of the $P_{2r}Qr$ in terms of the wave vector qa. Figure 4 shows that whatever the wave vector qa taken between 0 and π, the product $P_{2r}Qr \geq 0$ for $\sigma = \sigma^+$ (see Fig. 4a) and $P_{2r}Qr \leq 0$ for $\sigma = \sigma^-$ (see Fig. 4b). In the following, since we are looking for the bright-like soliton, which describes very well the situation studied in this paper (see Eq. (19)), we restrict ourselves to the case $P_{2r}Qr > 0$. In doing so, the wave vector should be selected, such as $qa \leq 2\pi/5$.

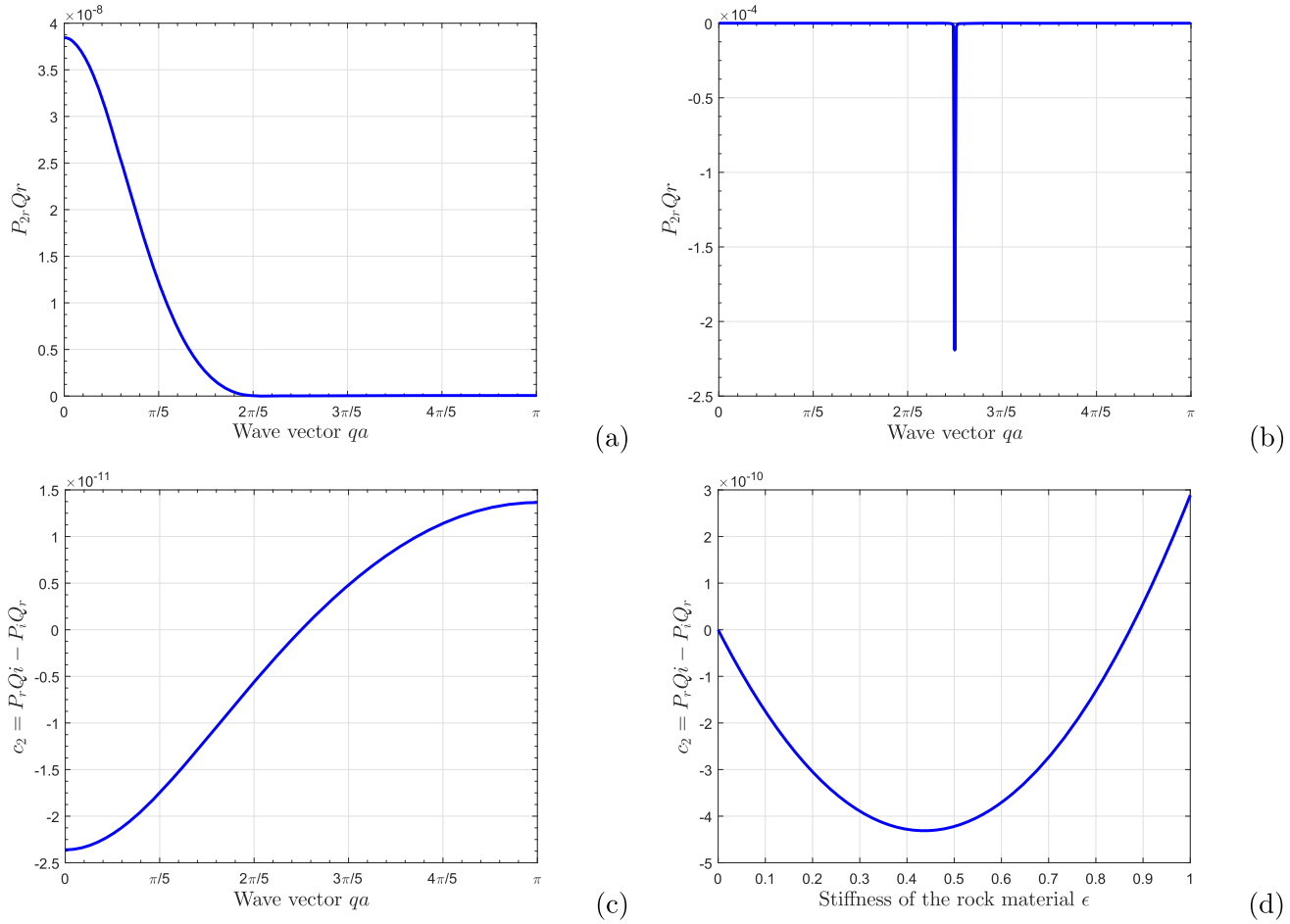

Fig. 4 Schematic representation of some parameters involved in the solution of the CGL equation (Eq. (19)). The product P_2r Q_r in terms of wave vector qa for $\theta = \pi/8$ and $\epsilon = 0.01$. Panel (**a**) for $\sigma = \sigma^+$; panel (**b**) for $\sigma = \sigma^-$; parameter c_2 panel (**c**). In panel (**d**), the evolution of the parameter c_2 is presented in terms of the stiffness of the rock material ϵ for $\theta = \pi/8$ and $qa = \frac{\pi}{6}$

The parameters ω_r, v_{gr}, and Γ found, respectively, in Eq. (18), Eq. (19), and Eq. (21) are the dispersion relation, the group velocity, and the damping coefficient of the soliton solution. These are plotted in Fig. 5. According to this graph, in addition to being positive, all these parameters are the increasing function of the wave vector.

Equation (20) is a non-conservative soliton solution of a bright-like type, representing the envelope wave soliton. By assuming normalized time such as $t \to \tau$, the soliton solution of Eq. (16) is, therefore, obtained from Eqs. (17), (18), (19), and (20), in the form

$$v_n = 2F_{1,n}\cos\Theta + 2F_{1,n}^2\Big[BC\cos(2\Theta) - DC\sin(2\Theta) - \epsilon\alpha_2\,\mathrm{e}^{2\chi t}\Big], \tag{21}$$

where

$$F_{1,n} = f_\varepsilon\,\mathrm{sech}\left[L_\varepsilon(na - v_{g,r}t)\right], \quad f_\varepsilon = f_{0,\varepsilon}\,\mathrm{e}^{-\Gamma t} \quad f_{0,\varepsilon} = \varepsilon f_0 = U_e\sqrt{\frac{1-2\mu}{2P_{2,r}\,Q_r}}, \quad U_e = \varepsilon u_e,$$

$$L_\varepsilon = L_{0,\varepsilon}\,\mathrm{e}^{-\gamma_{0,\varepsilon}t}, \quad L_{0,\varepsilon} = \sqrt{\frac{Q_r}{2P_{2,r}}}f_{0,\varepsilon}, \quad \Omega_\varepsilon = \omega_r - \varpi_\varepsilon, \quad \varpi_\varepsilon = P_{1,r}L_\varepsilon^2$$

$$\Theta = qna + \sigma\ln|\,\mathrm{sech}\left[L_\varepsilon(na - v_{g,r}t)\right]| - \Omega_\varepsilon t, \quad \Gamma = \gamma_{0,\varepsilon} + \chi, \quad \gamma_{0,\varepsilon} = P_{1,i}L_{0,\varepsilon}^2.$$

From Eq. (21), one has the time-dependent expression of the "effective" amplitude $A_\varepsilon(t)$, width $\aleph_\varepsilon(t)$, and frequency $\nu_\varepsilon(t)$ of the soliton solution, respectively, such as,

$$A_\varepsilon(t) = 2f_\varepsilon\Big[1 + f_\varepsilon\Big(BC - DC - \epsilon\alpha_2\,\mathrm{e}^{2\chi t}\Big)\Big], \quad \aleph_\varepsilon(t) = \frac{2\pi}{L_\varepsilon}, \quad \nu_\varepsilon(t) = \frac{\Omega_\varepsilon}{2\pi}. \tag{22}$$

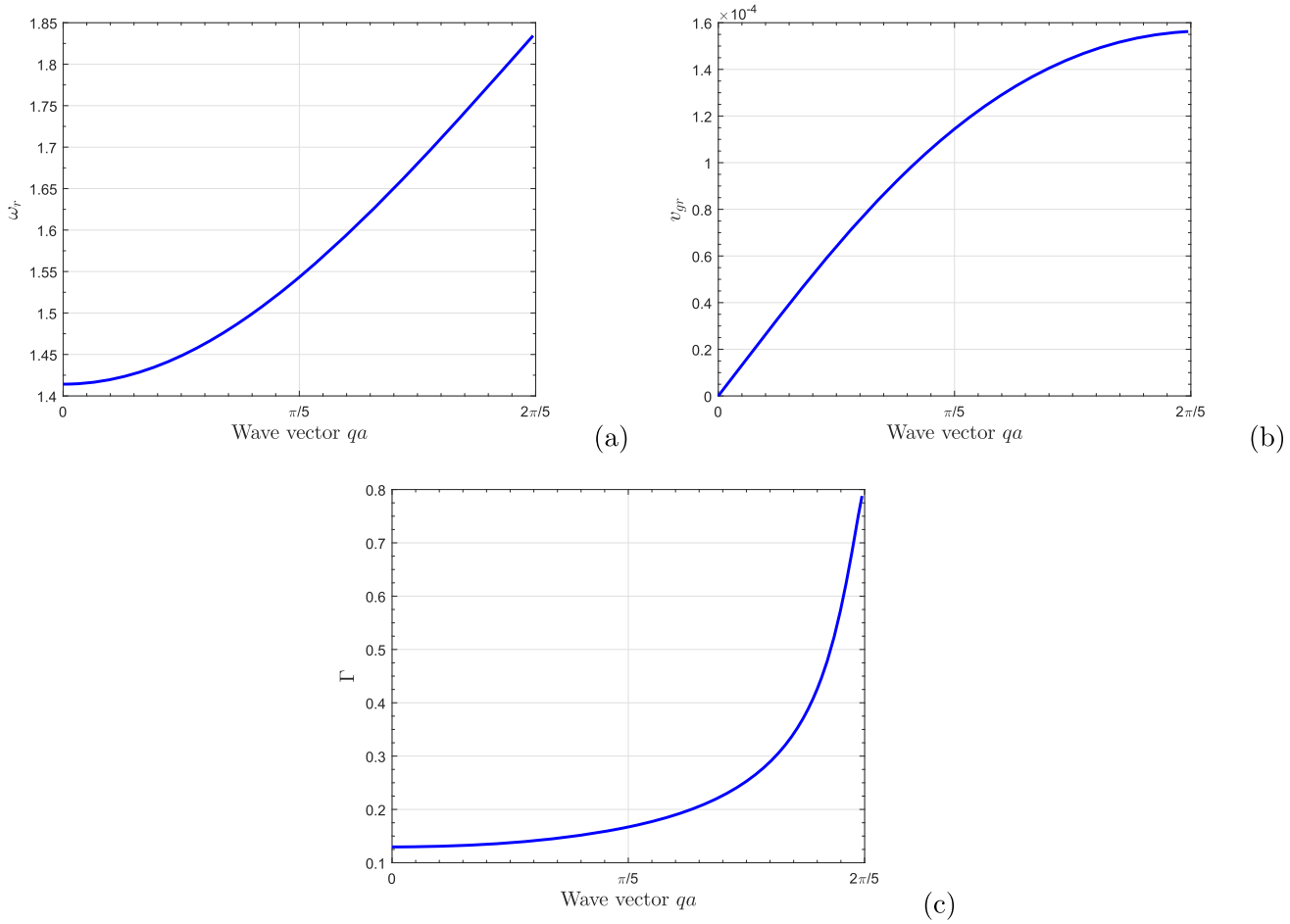

Fig. 5 Schematic representation of some parameters of the soliton solution in terms of wavenumber qa. Panel (**a**) the angular frequency, panel (**b**) the group velocity, and panel (**c**) the global damping parameter, for $\theta = \pi/8$ and $\epsilon = 0.01$

The width of the soliton represents the "bandwidth" of the earthquake, i.e. the area covered by the earthquake. The amplitude is related to the magnitude of the earthquake, while the frequency is related to the speed with which the blocks vibrate. In Figs. (6) and (7), the amplitude $A_\varepsilon(t)$, width $\aleph_\varepsilon(t)$, and frequency $\nu_\varepsilon(t)$ are plotted in terms of the wave vector as a function of normalized time (see Fig. 6) and in terms of the stiffness of rock material ϵ (see Fig. 7). We observe in Fig. 6 that, while the amplitude and the frequency of the soliton are decreasing functions of time, its width is an increasing function. Furthermore, in Fig. 7, we noticed a monotonic variation of the above parameters up to a certain value of $\epsilon_0 = 0.45$. Then, when ϵ exceeds this value, the variation changes direction but remains monotonic up to a critical value of $\epsilon_{cr} \approx 0.87$. Around this critical value, these parameters exhibit unexpected, inconsistent, and asymptotic behaviours, with limits that tend toward $+\infty$. That is, the right and left limits at ϵ_{cr} are completely different for each of the parameters. This abnormal and unexpected behaviour shows that ϵ_{cr} corresponds to the value of the stiffness for which the rock crashes [35]. Thus, in the rest of the paper, we restrict ourselves to $\epsilon \leq \epsilon_0$, for which the amplitude and the angular frequency decrease while the width increases. In other words, when rock reaches from dilatation to contraction, the bandwidth of the earthquakes increases, while its magnitude decreases.

It is important to notice here that although the parameters ϵ (see Eq. (6)) and ε (see Eq. (17)) are all small real numbers, they are not equal ($\varepsilon \neq \epsilon$) because the origins of both parameters are physically different. ϵ is an intrinsic parameter related to the elastic properties of rock material, for which stiffness increases from dilation to contraction. Such behaviour is well described by the cubic and quadratic terms in the stiffness forces $F_n^{(1)}$ [13], for which the value is adjusted by ϵ. That is, for $\epsilon \longrightarrow 0$, the rock material is in the dilation state (the nonlinear effects can be neglected), while for $\epsilon \longrightarrow 1$, the rock material is in the contraction state (the nonlinear effects are very important). Regarding ε, it is just a number coming from the mathematical tools and related to the small-amplitude approximation used. However, while ϵ remains in the equations, because allowing to adjust the nonlinearity of the system, ε disappears, absorbed in the arbitrary carrier wave velocity $U_e = \varepsilon u_e$ and related wave amplitude $f_{0,\varepsilon} = \varepsilon f_0$ (see Eq. (21)).

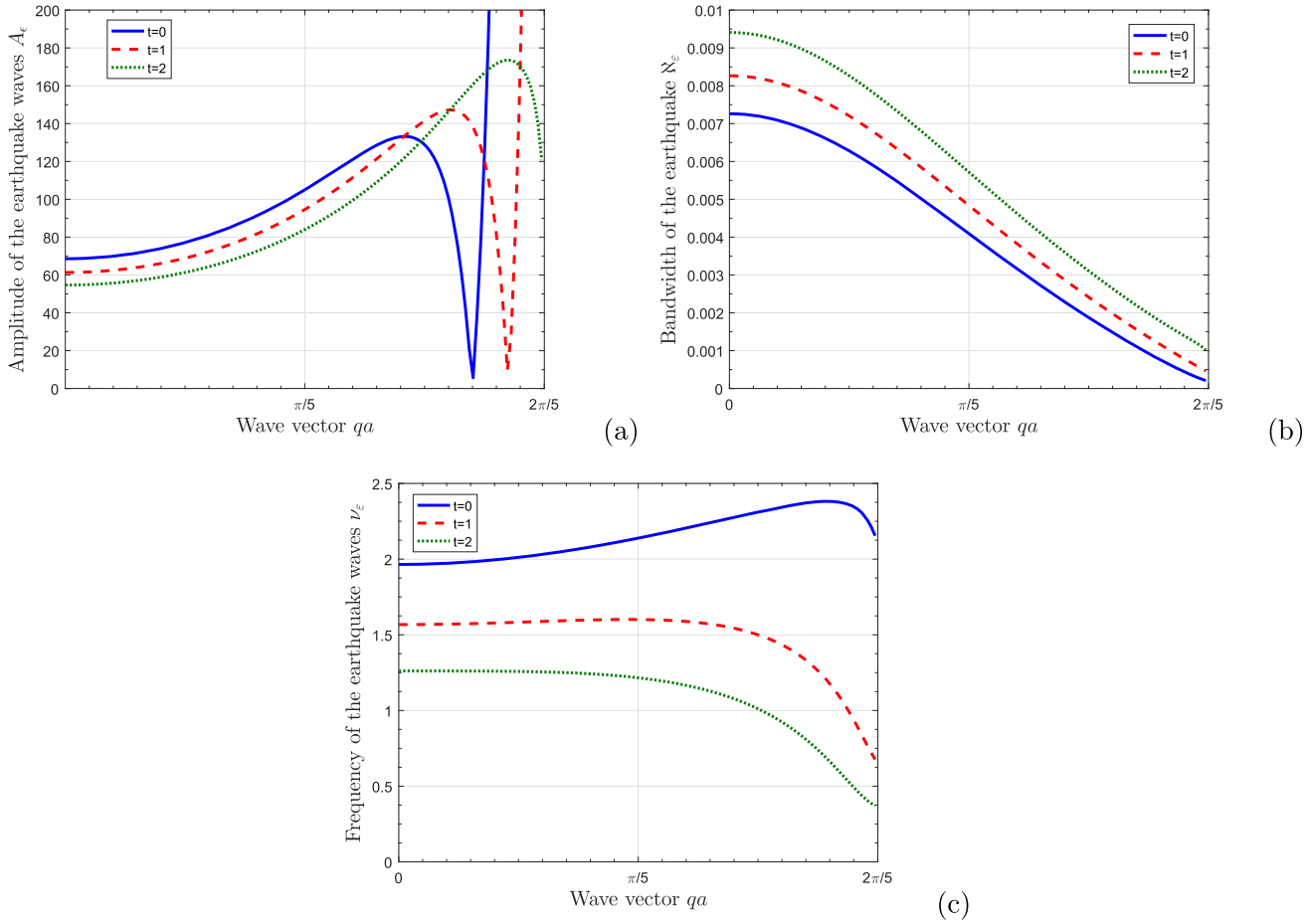

Fig. 6 Schematic representation of some parameters of the soliton solution in terms of wavenumber qa. Panel (**a**) the amplitude, panel (**b**) the bandwidth, and panel (**c**) the frequency, for $\theta = \pi/8$ and $\epsilon = 0.01$

The final soliton solution of the equation of motion (see Eq. (12)) is, therefore, obtained by considering Eqs. (13), (14), and (21),

$$x_n(t) = 2F_{1,n}\cos\Theta + 2F_{1,n}^2\Big[BC\cos(2\Theta) - DC\sin(2\Theta) - \alpha_2\,\mathrm{e}^{2\chi t}\Big] + \frac{1}{2}\Big[v_1 + \Big(p_1 - \beta r_1 u\Big)g\sin\theta\Big]. \tag{23}$$

3.2 Linear solution of the equation of motion

In this section, we focus on the linear effects for which $\epsilon = 0$. Thus, Eq. (16) becomes,

$$\ddot{u}_n = K_1\Big(u_{n+1} - 2u_n + u_{n-1}\Big) - 2u_n + \gamma_1^{hy}\Big(\dot{u}_{n+1} - 2\dot{u}_n + \dot{u}_{n-1}\Big) + \gamma_1\dot{u}_n, \tag{24}$$

where u_n represents the linear wave propagating in the earth crust during the ground shaking.

By assuming the wave solution on the form,

$$u_n = G_n\,\mathrm{e}^{\,\mathrm{i}\theta_n} + G_n^*\,\mathrm{e}^{\,-\mathrm{i}\theta_n}, \quad \theta_n = qan - \omega t, \tag{25}$$

in the co-moving reference frame at the velocity v_g, setting $x = \varepsilon(na - v_g t)$ and $\tau = \varepsilon^2 t$. One obtains,

$$\mathrm{i}\,\frac{\partial G}{\partial \tau} + (P_r + \mathrm{i}\,P_i)\frac{\partial^2 G}{\partial x^2} = 0. \tag{26}$$

Equation (26) is the well-known complex linear Schrodinger (CLS) equation, that is, the linear Schrodinger equation with complex coefficients for which the wave solution is taken in the form,

$$G(x,\tau) = g(\tau)\,\mathrm{e}^{\,\mathrm{i}(kx - h(\tau))}, \tag{27}$$

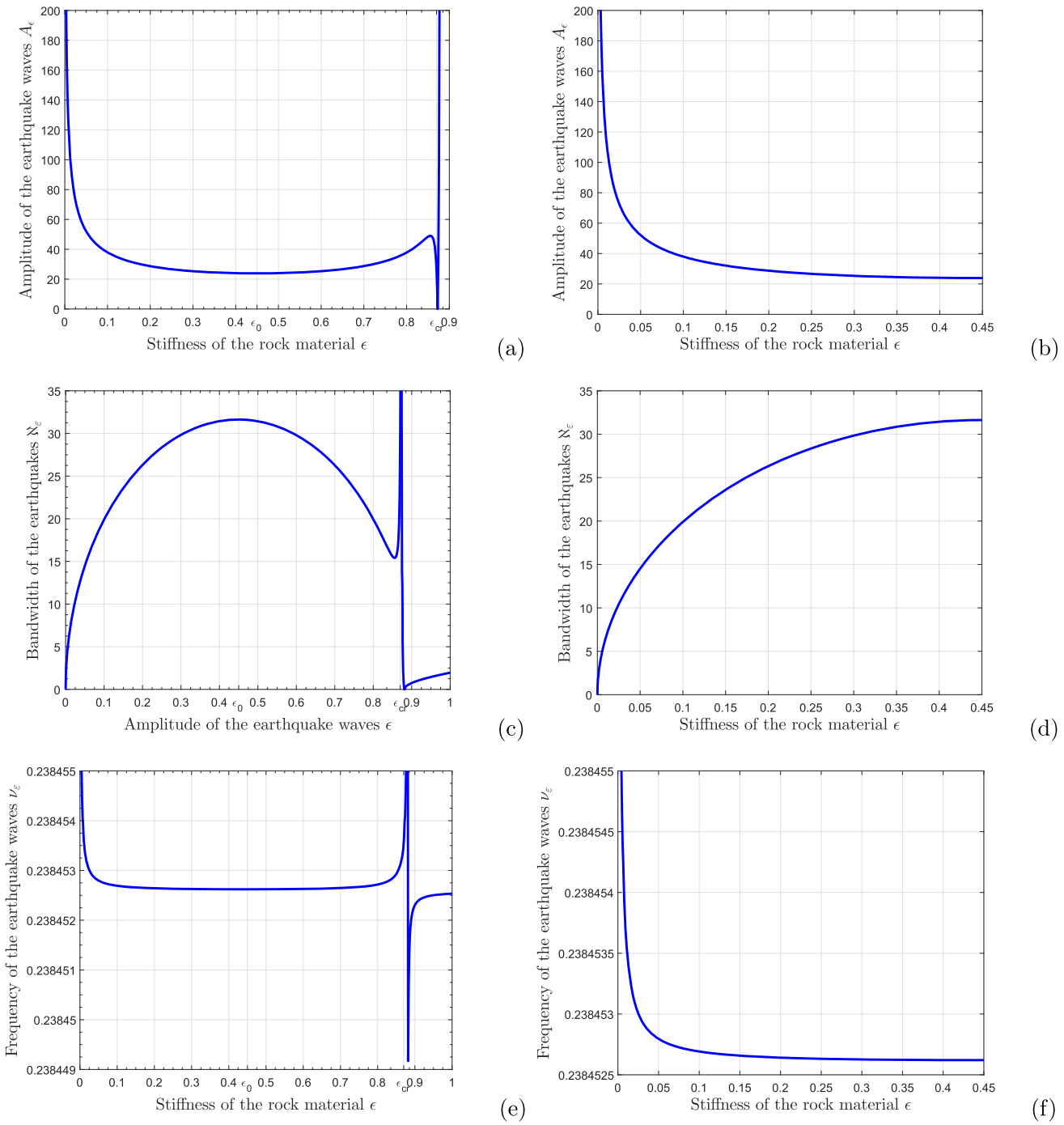

Fig. 7 Schematic representation of some parameters of the soliton solution in terms of stiffness of the rock material ϵ. Panel (**a**) and (**b**) the amplitude, panel (**c**) and (**d**) the bandwidth, and panel (**e**) and (**f**) the frequency for $\theta = \pi/8$, $qa = \frac{\pi}{6}$

with $g(\tau)$ and $h(\tau)$ are the real functions of variable τ. While h is the wavenumber, $\frac{\mathrm{d}\, h(\tau)}{d\tau}$ is assumed to be the angular frequency of the wave. Equation (27) in Eq. (26) gives,

$$G(x,\tau) = A_0\, \mathrm{e}^{\,P_i k^2 \tau}\, \mathrm{e}^{\,\mathrm{i}(kx - P_r k^2 \tau)}, \tag{28}$$

One should remember that the present CLS equation was obtained in the co-moving reference frame at the velocity $|v_g|$. For this, one has set $x = \varepsilon(na - |v_g|t)$ and rescaled the time such as $\tau = \varepsilon^2 t$. In addition, the parameters A_0, k, and $\varepsilon \ll 1$ are arbitrary real numbers; thus, without loss of generality, one assumes $A_0 \to \varepsilon A_0$ and $k \to \varepsilon k$, with A_0 and k being the amplitude and wavenumber

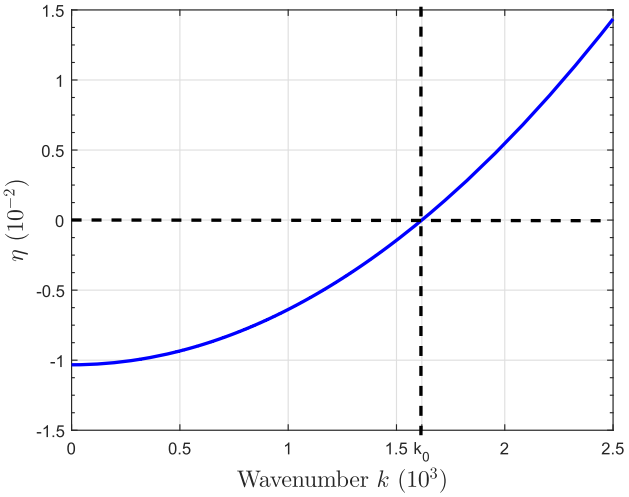

Fig. 8 Schematic representation of the parameter η as the function of the wavenumber k, for $qa = \frac{\pi}{6}$, $\theta = \pi/8$

of the wave. Then, taking into consideration all of this, the final wave solution of the linear equation of motion (see Eq. (24)) is easily obtained by considering Eqs. (25), (28), and (21). Thus, one has

$$u_n(t) = 2A_0\, \mathrm{e}^{-\eta t} \cos(Qna - \Omega t), \tag{29}$$

with

$$\eta = |P_i|k^2 + \chi, \quad Q = q + k, \quad \Omega = \omega_r + P_r k^2 + k v_{g,r},$$

where P_r, P_i, ω, v_g, and χ are given in Eqs. (18) and (19). Equation (29) is the dissipative plane wave solution of the linear equation of motion. It represented the linear earthquake waves propagating in the dilated rock material during an earthquake.

In Fig. 8, the snapshot of the evolution of the parameter η in terms of wavenumber k is presented. From this picture, it is observed that η can be negative, positive, or zero depending on the value of the wavenumber k.

If $\eta < 0$, which corresponds to $k < k_0$, with $k_0 = -\frac{\chi}{|P_i|} \approx 1.6172.10^3$, the amplitude of plane seismic waves generated in the Earth's crust by an earthquake increases exponentially during their propagation. The energy induced by these waves increases in a similar way. The propagation of such waves would be infinite, and the damage caused by such an earthquake would be very destructive and could even call into question the existence of life on Earth. For $\eta = 0$, which refers to $k = k_0$, we observe seismic waves propagating with a constant amplitude and in an infinite manner. This situation is similar to the one described above. For $\eta > 0$, which corresponds to $k > k_0$, the amplitude of the wave decreases exponentially in time, leading to a decrease in the induced energy in the same proportions. This corresponds to the commonly accepted physical reality experimentally observed. Thus, in the rest of our work, we will limit ourselves to the case $\eta > 0$, which imposes a very selective choice of wavenumber k, such that $k > k_0$. In this case, η behaves as a damping term that damps out the amplitude of the wave during its propagation.

4 Numerical investigations

Let us remember here that the theoretical results clearly show that the parameters of the soliton, which deal with the positive values of the damping term within the motion (see Fig. 5c and Fig. 8), evolve differently over time. While the amplitude and angular frequency decrease, the width increases (see Fig. 6). This clearly shows that the system is modulationnally unstable.

Our objective in this part of our work is to numerically check the properties of the earthquake waves represented by the bright-like soliton (as well as the plane wave) solution of the CGL (as well as the CLS) equation. The correctness, stability, robustness, and long-term evolution of the analytical solutions are also explored. Doing so, the numerical simulations of the discrete equations of motion Eq. (16) (as well as Eq. (24)) are done by using the analytical solution Eq. (21) (as well as Eq. (29)) as initial conditions. A series of numerical experiments is involved over a very long time with a large lattice, using the fourth-order Runge–Kutta scheme with periodic boundary conditions. The total energy of the system is preserved to a good accuracy over a complete run by an appropriate time step chosen as Δt=10^{-5} normalized time units (t.u.). We focus on the shape, width, and amplitude of the propagating wave at a given time. The numerical parameters used for simulations are those used in the theory.

Figure 9 presents the 3D space–time evolution of the envelope soliton, while in Fig. 10 presents the 3D space–time evolution of the soliton solution. As predicted by the theory (see Fig. 6a and Fig. 6b), when the soliton propagates, its amplitude and width exhibit an exponential diminution and growth, respectively. In Fig. 10, the snapshot of the soliton and its envelope is shown at four different time positions. The curves not only show the decrease in the amplitude and the increase in the width of the soliton over

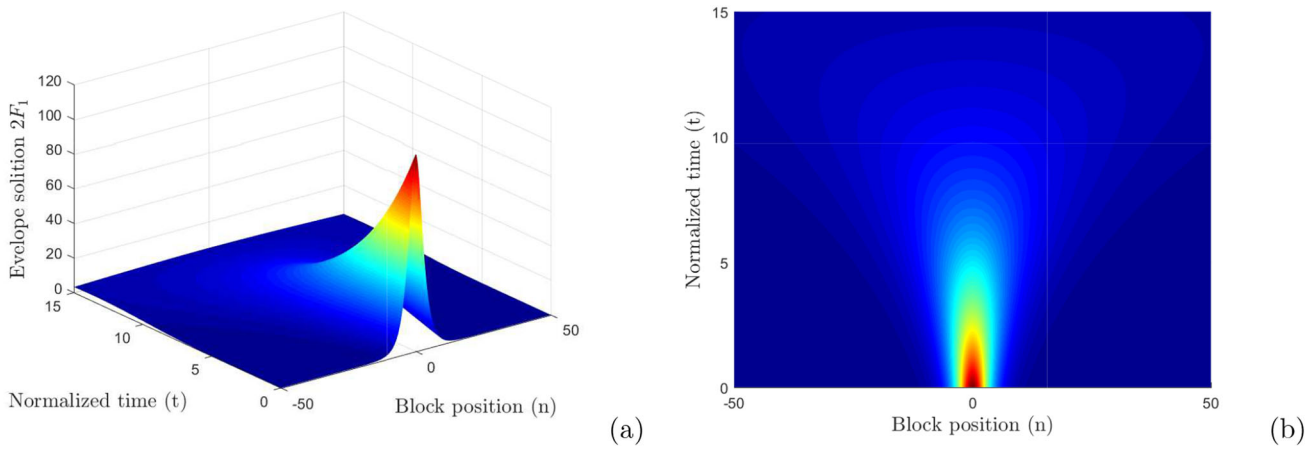

Fig. 9 Three-*dimensional* numerical simulations of the nonlinear envelope soliton, for $qa = \frac{\pi}{6}$, $\theta = \pi/8$, and $\epsilon = 0.01$

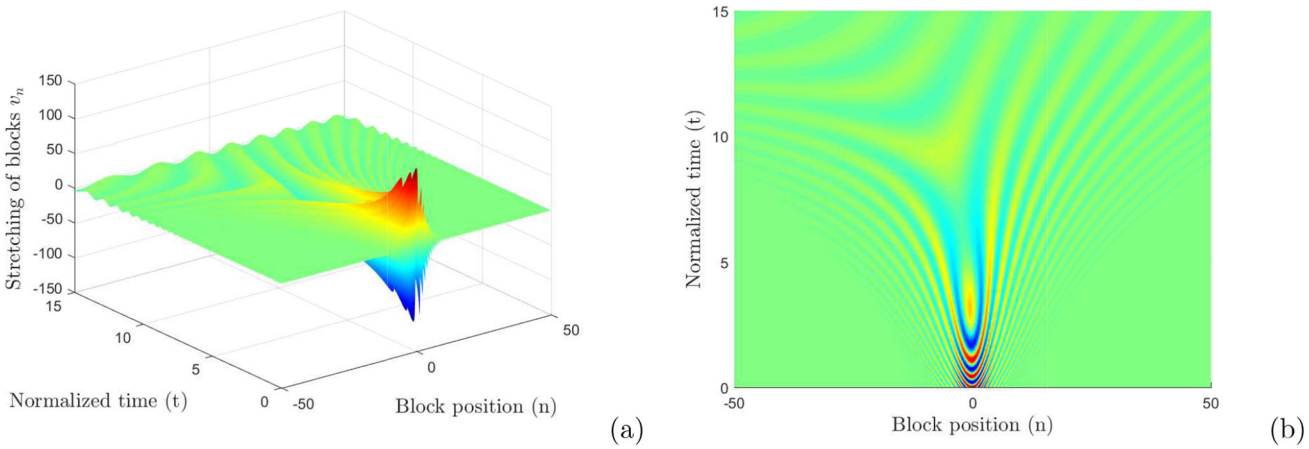

Fig. 10 Three-*dimensional* numerical simulations of the evolution of nonlinear stretching of the blocks, for $qa = \frac{\pi}{6}$, $\theta = \pi/8$, and $\epsilon = 0.01$

time, but also show the decrease in the angular frequency of vibration of the latter. This shows that the magnitude, the area covered, and the frequency of the ground shaking depend on friction.

Figure (12) (as well as Fig. 13) represents the evolution of the nonlinear (as well as linear) waves and the related phase portraits for different values of the stiffness of the rock material. Although the decrease in wave amplitude is observed over time as predicted by theory, this decrease is also observed when ϵ evolves. In the nonlinear situation ($\epsilon \neq 0$), the lines show that the waves that propagate with a constant shape (see Fig. 12, panels (a), (c), and (e)). Moreover, as predicted by theory, any system governed by the CGL equation exhibits chaotic behaviour; the phase portraits (see Fig. 12, panels (b), (d), and (f)) show chaotic-like behaviour that becomes more pronounced towards the end of the earthquake propagation. In addition, the linear propagation exhibits coherent behaviour from the beginning to the end of their propagation (see Fig. 13b). This means that the elasticity of the rock material does not affect the shape of earthquake waves.

The results of our numerical experiments, as depicted in Fig. 9, Fig. 10, Fig. 11, Fig. 12, and Fig. 13, show good agreement with theoretical results, showing that our analytical solution is robust and suitable to predict the nonlinear properties of earthquake waves propagating along the earth crust.

5 Conclusion

In this work, we have investigated the propagation of nonlinear earthquake waves along the Earth crust. We have used an extended version of the Burridge–Knopoff model, including the hydrodynamic damping forces, the nonlinear stiffness of the elasticity of the rock material, and empirical friction forces approved experimentally. The blocks are placed on a downward slope with an angle of θ with respect to the horizontal line. The model, reduced to a nonlinear wave equation, was shown to induce landslides. A link between floor velocity and earthquake-induced landslides is highlighted, demonstrating that any earthquake induces ground displacement, regardless of slope. The importance of this displacement depends on the slope angle and duration of the ground

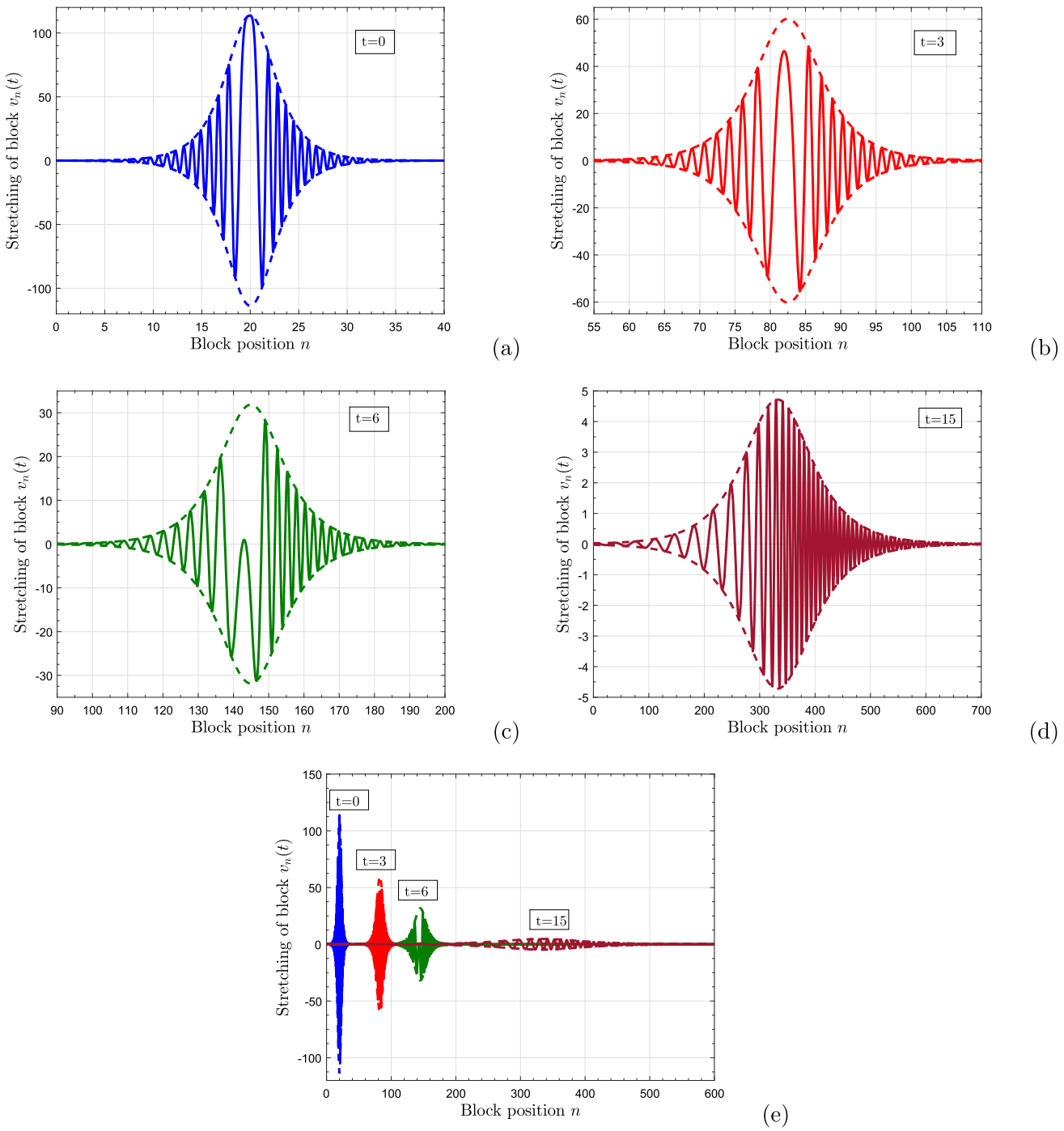

Fig. 11 Two-*dimensional* snapshot of the numerical evolution of the nonlinear stretching of the blocks at different time positions, for $qa = \frac{\pi}{6}$, $\theta = \pi/8$, and $\epsilon = 0.01$. The dash lines represent the envelope soliton, while the solid lines represent the blocks stretching

shaking. In the semi-discrete approximation, the wave equation was reduced to the CGL equation, allowing a bright-like soliton solution, which represented the evolution of the earthquake wave along the ground. The propagation of the wave was found to be stable, and theoretical predictions were confirmed by a series of numerical experiments with good accuracy. The results clearly show that any propagation of earthquake waves triggers a landslide, with disastrous damage to buildings, human and animal lives, and economic activities. Also, as experimentally expected, it is found that the residual displacement of the block rocks increases with the slope angle. Therefore, the results present in this paper are very relevant, as they can explain and predict the observations of natural earthquakes. The case at hand is devoted to an idealized description of rock blocks, where the blocks have the same size, the soil is homogeneous, and other sources of landslides are neglected. Otherwise, the real ground is complex. It involves inhomogeneities

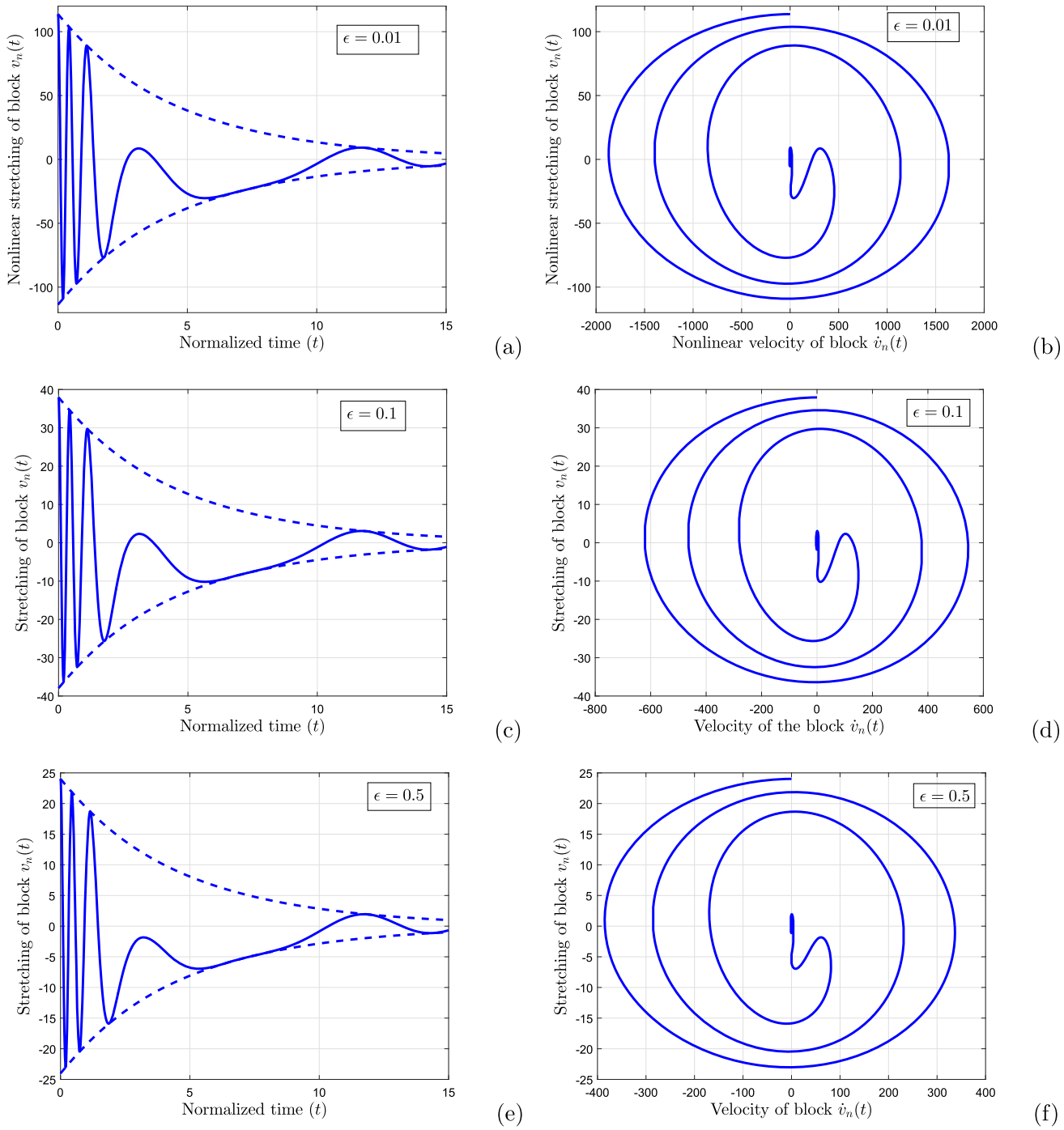

Fig. 12 Two-*dimensional* numerical evolution of the nonlinear stretching of the blocks and related phase portraits, for different values of the stiffness of the rock material ϵ, $qa = \frac{\pi}{6}$, and $\theta = \pi/8$. The dash lines represent the envelope soliton, while the solid lines represent the blocks stretching

and many other geological factors that are not included in the present model. In a forthcoming work, we propose to study the earth shaking with some geological factors such as geothermic, external sources of landslides, or ground inhomogeneities.

We have used an extended version of the Burridge–Knopoff model, including the hydrodynamic damping forces, the nonlinear stiffness of the elasticity of the rock material, and empirical friction forces approved experimentally. The blocks are placed on a downward slope with an angle of θ with respect to the horizontal line. The model, reduced to a nonlinear wave equation, was shown to induce landslides. A link between floor velocity and earthquake-induced landslides is highlighted, demonstrating that any earthquake induces ground displacement, regardless of slope. The importance of this displacement depends on the slope angle and duration of the ground shaking. In the semi-discrete approximation, the wave equation was reduced to the CGL equation, allowing

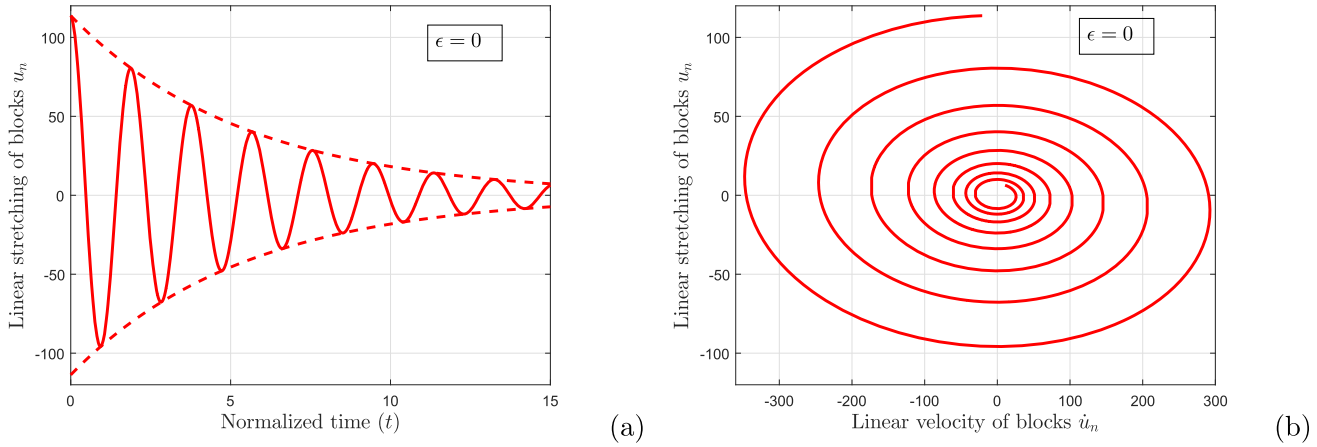

Fig. 13 Two-*dimensional* numerical evolution of the linear stretching of the blocks and related phase portraits, for $\epsilon = 0$ $A_0 = 2f_{0,\varepsilon}$, $\theta = \pi/8$, and $qa = \pi/6$

a bright-like soliton solution, which represented the evolution of the earthquake waves along the ground. In the linear limit, the system is found to be governed by the plane wave solution of the CLS equation. The propagation of the waves was found to be stable, and theoretical predictions were confirmed by a series of numerical experiments with good accuracy. The results clearly show that any propagation of earthquake waves triggers a landslide, with disastrous damage to buildings, human and animal lives, and economic activities. Also, as experimentally expected, it is found that the residual displacement of the block rocks increases with the slope angle. Therefore, the results present in this paper are very relevant, as they can explain and predict the observations of natural earthquakes. The case at hand is devoted to an idealized description of rock blocks, where the blocks have the same size, the soil is homogeneous, and other sources of landslides are neglected. Otherwise, the real ground is complex. It involves inhomogeneities and many other geological factors that are not included in the present model. In a forthcoming work, we propose to study the earth shaking with some geological factors such as geothermic, external sources of landslides, or ground inhomogeneities.

Data Availability Statement No datasets were generated or analysed during the current study.

Appendix A Derivation of the CGL equation using the multiple scale expansion method in the semi-discrete approximation

The steps for getting the CGL equation (Eq. (19)) from Eq. (16) are explained in this section, since the method was briefly mentioned in the main paper (see Sec. 3).

The solution of Eq. (16) is assumed in the form of Eq. (17), rewritten here for our own convenience, such as

$$v_n(t) = \varepsilon\psi_n(t), \tag{A1}$$

with

$$\psi_n(t) = \left[F_{1,n}\,\mathrm{e}^{\,\mathrm{i}\theta_n} + F_{1,n}^{*}\,\mathrm{e}^{\,-\mathrm{i}\theta_n}\right] + \varepsilon\left[F_{0,n} + \left(F_{2,n}\,\mathrm{e}^{\,2\mathrm{i}\theta_n} + F_{2,n}^{*}\,\mathrm{e}^{\,-2\mathrm{i}\theta_n}\right)\right], \tag{A2}$$

where $\theta_n = qan - \omega t$.

Equation (A1) in Eq. (16) gives,

$$\ddot{\psi}_n = K_1(\psi_{n+1} - 2\psi_n + \psi_{n-1}) - 2\left[\psi_n + \varepsilon(\epsilon\alpha_2)\psi_n^2 + \varepsilon^2(\epsilon\alpha_3)\psi_n^3\right] + \gamma_1^{hy}(\dot{\psi}_{n+1} - 2\dot{\psi}_n + \dot{\psi}_{n-1}) + \gamma_1\dot{\psi}_n. \tag{A3}$$

From Eq. (A2) one has,

$$\psi_n^2 = F_{1,n}^2 e^{2i\theta} + 2|F_{1,n}|^2 + \varepsilon\left[2F_{0,n}F_{1,n}e^{i\theta} + 2F_{2,n}F_{1,n}^{*}e^{i\theta}\right], \quad \psi^3 = 3|F_{1,n}|^2 F_{1,n}e^{i\theta}. \tag{A4}$$

We set new space and time scale variables, $z_j = \varepsilon^j z$ and $T_j = \varepsilon^j t$ [39]. The solution $v_n \longrightarrow v(z, t)$ is found as a perturbation series of functions. Thus, one assumes

$$v(z,t) = \sum_{j=1}^{\infty} \varepsilon^j \psi_j(z_0, z_1, z_2, ..., T_0, T_1, T_2, ...), \tag{A5}$$

where z_j and T_j are independent parameters.

The perturbation series of the operator deduced from the independent variables $z_j(z_0 = z,\ z_1 = \varepsilon z,\ z_2 = \varepsilon^2 z,\ ...)$ and $T_j(T_0 = t,\ T_1 = \varepsilon t,\ T_2 = \varepsilon^2 t,\ ...)$ are easily obtained for the time derivative and for the spatial derivative,

$$\frac{\partial}{\partial t} = \frac{\partial}{\partial T_0} + \varepsilon\frac{\partial}{\partial T_1} + \varepsilon^2\frac{\partial}{\partial T_2} + ..., \quad \frac{\partial}{\partial z} = \frac{\partial}{\partial z_0} + \varepsilon\frac{\partial}{\partial z_1} + \varepsilon^2\frac{\partial}{\partial z_2} + ... \tag{A6}$$

The main feature of this technique is that the multidimensional space generated by the new sets of variables z_j and T_j comes from the physical line [39] and permits us to impose particular conditions on the system, such as the uniform convergence of the asymptotic expansion for small values of ε. The amplitudes F_1, F_0, and F_2 are supposedly to be independent of the "fast" variables t and z (as well as T_0 and z_0). Instead, they assume to depend only on the "slow" variables $z_1 = \varepsilon z$, $z_2 = \varepsilon^2 z$, ..., $T_1 = \varepsilon t$, $T_2 = \varepsilon^2 t$, ... Doing so, the continuum limit approximation, by using a Taylor expansion up to the second order in ε, of these amplitudes is obtained, respectively, for spatial derivatives,

$$F_{j,n\pm1} = F_j \pm (\varepsilon a)\frac{\partial F_j}{\partial z_1} \pm (\varepsilon a)^2\frac{\partial F_j}{\partial z_2} + \frac{1}{2}(\varepsilon a)^2\frac{\partial^2 F_j}{\partial z_1^2} + O(\varepsilon a)^3, \tag{A7}$$

and for temporal derivatives.

$$\frac{\partial F_j}{\partial t} = \varepsilon\frac{\partial F_j}{\partial T_1} + \varepsilon^2\frac{\partial F_j}{\partial T_2}, \quad \frac{\partial^2 F_j}{\partial t^2} = \varepsilon^2\frac{\partial^2 F_j}{\partial T_1^2} + O(\varepsilon^3), \tag{A8}$$

with $j = 0,\ 1,\ 2$.

One should remember that only the amplitudes are treated in the continuum limits; the carrier waves are kept discrete. For instance,

$$\psi_{n\pm1} = F_{1,n\pm1}\,\mathrm{e}^{\,\mathrm{i}\theta_{n\pm1}} + \varepsilon\left[F_{0,n\pm1} + F_{2,n\pm1}\,\mathrm{e}^{\,\mathrm{i}2\theta_{n\pm1}}\right]. \tag{A9}$$

While the amplitudes $F_{j,n\pm1}$ are developed according to Eq. (A7), the carrier waves are treated such as,

$$\mathrm{e}^{\,\pm j\,\mathrm{i}\theta_{n\pm1}} = \mathrm{e}^{\,\pm j\,\mathrm{i}qa}\,\mathrm{e}^{\,j\,\mathrm{i}\theta_n}. \tag{A10}$$

With this in mind, Eq. (A10), Eq. (A9), Eq. (A8), and Eq. (A7) together with Eq. (A2) give

$$\begin{aligned}
\dot{\psi} &= -\mathrm{i}\omega F_1\,\mathrm{e}^{\,\mathrm{i}\theta_n} + \varepsilon\left[\frac{\partial F_1}{\partial T_1}\,\mathrm{e}^{\,\mathrm{i}\theta_n} - 2\,\mathrm{i}\omega F_2\,\mathrm{e}^{\,2\mathrm{i}\theta_n}\right] + \varepsilon^2\left[\frac{\partial F_1}{\partial T_2}\,\mathrm{e}^{\,\mathrm{i}\theta_n} + \frac{\partial F_2}{\partial T_1}\,\mathrm{e}^{\,2\mathrm{i}\theta_n}\right],\\
\ddot{\psi} &= -\omega^2 F_1\,\mathrm{e}^{\,\mathrm{i}\theta_n} + \varepsilon\left[-2\,\mathrm{i}\omega\frac{\partial F_1}{\partial T_1}\,\mathrm{e}^{\,\mathrm{i}\theta_n} - 4\omega^2 F_2\,\mathrm{e}^{\,2\mathrm{i}\theta_n}\right]\\
&\quad + \varepsilon^2\left[\frac{\partial^2 F_1}{\partial T_1^2}\,\mathrm{e}^{\,\mathrm{i}\theta_n} - 2\,\mathrm{i}\omega\frac{\partial F_1}{\partial T_2}\,\mathrm{e}^{\,2\mathrm{i}\theta_n} - 4\,\mathrm{i}\omega\frac{\partial F_2}{\partial T_1}\,\mathrm{e}^{\,2\mathrm{i}\theta_n}\right],
\end{aligned} \tag{A11}$$

$$\begin{aligned}
\psi_{n+1} - 2\psi_n + \psi_{n-1} &= -4\sin^2\left(\frac{qa}{2}\right)F_1\,\mathrm{e}^{\,\mathrm{i}\theta_n} + \varepsilon\left[2\,\mathrm{i}a\sin(qa)\frac{\partial F_1}{\partial z_1}\,\mathrm{e}^{\,\mathrm{i}\theta_n} - 4\sin^2(qa)\,\mathrm{e}^{\,\mathrm{i}2\theta_n}\right]\\
&\quad + \varepsilon^2\left[2\,\mathrm{i}a^2\sin(qa)\frac{\partial F_1}{\partial z_2}\,\mathrm{e}^{\,\mathrm{i}\theta_n} + a^2\cos(qa)\frac{\partial^2 F_1}{\partial z_1^2}\,\mathrm{e}^{\,\mathrm{i}\theta_n} - 2\,\mathrm{i}a\sin(2qa)\frac{\partial F_2}{\partial z_1}\,\mathrm{e}^{\,2\mathrm{i}\theta_n}\right],\\
\dot{\psi}_{n+1} - 2\dot{\psi}_n + \dot{\psi}_{n-1} &= 4\,\mathrm{i}\omega\sin^2\left(\frac{qa}{2}\right)F_1\,\mathrm{e}^{\,\mathrm{i}\theta_n}\\
&\quad + \varepsilon\left[-4\sin^2\left(\frac{qa}{2}\right)\frac{\partial F_1}{\partial T_1}\,\mathrm{e}^{\,\mathrm{i}\theta_n} + 2a\omega\sin(qa)\frac{\partial F_1}{\partial z_1}\,\mathrm{e}^{\,\mathrm{i}\theta_n} + 8\,\mathrm{i}\omega\sin^2(qa)F_2\,\mathrm{e}^{\,2\mathrm{i}\theta_n}\right]\\
&\quad + \varepsilon^2\left[-4\sin^2(\frac{qa}{2})\frac{\partial F_1}{\partial T_2}\,\mathrm{e}^{\,\mathrm{i}\theta_n} + 2\,\mathrm{i}a\sin(qa)\frac{\partial}{\partial T_1}\left(\frac{\partial F_1}{\partial z_1}\right)\mathrm{e}^{\,\mathrm{i}\theta_n} - 4\sin^2(qa)\frac{\partial F_2}{\partial T_1}\,\mathrm{e}^{\,2\mathrm{i}\theta_n}\right.\\
&\quad \left. + 2a^2\omega\sin(qa)\frac{\partial F_1}{\partial z_2}\,\mathrm{e}^{\,\mathrm{i}\theta_n} - \mathrm{i}a^2\omega\cos(qa)\frac{\partial^2 F_1}{\partial z_1^2}\,\mathrm{e}^{\,\mathrm{i}\theta_n} + 4a\omega\sin(2qa)\frac{\partial F_2}{\partial z_1}\,\mathrm{e}^{\,2\mathrm{i}\theta_n}\right].
\end{aligned} \tag{A12}$$

We insert Eq. (A12), Eq. (A11), Eq. (A4), and Eq. (A2) into Eq. (A3) and collect the terms in $e^{j\,\mathrm{i}\theta_n}$ at different orders of ε^j, $j = 0,\ 1,\ 2$.

Thus, at the order ε^0, the terms in $e^{\,\mathrm{i}\theta_n}$ give

$$\omega = \omega_r + i\omega_i, \quad \omega_r = \sqrt{\omega_0^2 - \chi^2}, \quad \omega_i = -\chi, \tag{A13}$$

where

$$\chi = \frac{1}{2}\gamma, \quad \gamma = \gamma_1 - 4\gamma_1^{hy}\sin^2\left(\frac{qa}{2}\right), \quad \omega_0^2 = 2 + 4K_1\sin^2\left(\frac{qa}{2}\right), \tag{A14}$$

with ω_r, γ, and ω_0 being the angular frequency, the global damping coefficient, and the angular frequency without damping, respectively.

At the order ε^1, the terms without exponentials, the terms in $e^{(\mathrm{i}\theta_n)}$, and the terms in $e^{(2\,\mathrm{i}\theta_n)}$ give the relations,

$$F_0 = -2(\epsilon\alpha_2)|F_1|^2, \quad \frac{\partial F_1}{\partial T_1} + v_g \frac{\partial F_1}{\partial z_1} = 0, \quad F_2 = (BC + \mathrm{i}\, DC)F_1^2, \tag{A15}$$

with

$$\begin{aligned} &v_g = v_{gr} + i v_{gi}, \quad v_{gr} = \frac{a}{\omega_r}\Big(K_1 - \chi\gamma_1^{hy}\Big)\sin(qa), \quad v_{gi} = -a\gamma_1^{hy}\sin(qa), \varsigma = 2 + 4K_1\sin^2(qa) \\ &B = (4\omega_r - \varsigma) - 2\chi(2\chi - \gamma'), \quad D = \omega_r\big[4\chi + 2(2\chi - \gamma')\big], \quad \gamma' = \gamma_1 - 4\gamma_1^{hy}\sin^2(qa), \\ &C = \frac{2(\epsilon\alpha_2)}{B^2 + D^2}. \end{aligned} \tag{A16}$$

At the order ε^2, the terms $e^{(\mathrm{i}\theta_n)}$ give the equation of evolution of the envelope function, such as

$$\begin{aligned} \frac{\partial^2 F_1}{\partial T_1^2} - 2\,\mathrm{i}\,\omega\frac{\partial F_1}{\partial T_2} =& K_1\left[2\,\mathrm{i}\,a^2\frac{\partial F_1}{\partial z_2}\sin(qa) + a^2\cos(qa)\frac{\partial^2 F_1}{\partial z_1^2}\right] \\ &- 2\big[(\epsilon\alpha_2)(2F_0F_1 + 2F_2F_1^*) + 3(\epsilon\alpha_3)|F_1|^2F_1\big] \\ &+ \gamma^{hy}\left[-4\sin^2(qa)\frac{\partial F_1}{\partial T_2} + 2\,\mathrm{i}\,a\sin(qa)\frac{\partial}{\partial T_1}\left(\frac{\partial F_1}{\partial z_1}\right)\right. \\ &\left.+2a^2\omega\sin(qa)\frac{\partial F_1}{\partial z_2} - \mathrm{i}\,a^2\omega\cos(qa)\frac{\partial^2 F_1}{\partial z_1^2}\right] \\ &+ \gamma_1\frac{\partial F_1}{\partial T_2}. \end{aligned} \tag{A17}$$

In the co-moving reference frame, we set

$$\xi_j = z_j - v_g T_j, \quad \tau_j = T_j, \quad \texttt{with} \quad j = 1, 2. \tag{A18}$$

From Eq. (A18), one obtains temporal and spatial derivatives with respect to the new variables z_j and T_j,

$$\frac{\partial F_1}{\partial z_j} = \left(\frac{\partial \xi_j}{\partial z_j}\right)\frac{\partial F_1}{\partial \xi_j} + \left(\frac{\partial \tau_j}{\partial z_j}\right)\frac{\partial F_1}{\partial \tau_j}, \quad \frac{\partial F_1}{\partial T_j} = \left(\frac{\partial \xi_j}{\partial T_j}\right)\frac{\partial F_1}{\partial \xi_j} + \left(\frac{\partial \tau_j}{\partial T_j}\right)\frac{\partial F_1}{\partial \tau_j}. \tag{A19}$$

The differentiation of the amplitude F_1 with respect to the above new variables yields,

$$\frac{\partial F_1}{\partial z_2} = \frac{\partial F_1}{\partial \xi_2}, \quad \frac{\partial F_1}{\partial z_1} = \frac{\partial F_1}{\partial \xi_1}, \quad \frac{\partial F_1}{\partial T_1} = -v_g\frac{\partial F_1}{\partial \xi_1} + \frac{\partial F_1}{\partial \tau_1}, \quad \frac{\partial F_1}{\partial T_2} = -v_g\frac{\partial F_1}{\partial \xi_2} + \frac{\partial F_1}{\partial \tau_2}. \tag{A20}$$

We are looking for a solution independent of ξ_2; also from Eq. (A15), one has $\frac{\partial F_1}{\partial \tau_1} = 0$. Taking into account these considerations, from Eq. (A20), one has

$$\frac{\partial F_1}{\partial z_1} = \frac{\partial F_1}{\partial \xi_1}, \quad \frac{\partial F_1}{\partial T_1} = -v_g\frac{\partial F_1}{\partial \xi_1}, \quad \frac{\partial F_1}{\partial T_2} = \frac{\partial F_1}{\partial \tau_2}, \quad \frac{\partial^2 F_1}{\partial T_1^2} = v_g^2\frac{\partial^2 F_1}{\partial \xi_1^2}. \tag{A21}$$

Thus, using Eq. (A21) in Eq. (A17) and assuming new notation for the sake of simplicity, $\xi_1 = x$ and $\tau_2 = \tau$, allows us to Eq. (19). However, one should remember that while going from continuum to discrete, Eq. (A18) and Eq. (A5) show $x = \varepsilon(z - v_g t)$ and $\tau = \varepsilon^2 t$, with $z = an$. However, since v_g is a complex number, in the numerical simulation, we use its real part $v_{g,r}$.

References

1. S.A. Arsen'yev, L.V. Eppelbaum, T. Meirova, Earthquake processes: A view from synergetics and the theory of catastrophes. Pure Appl. Geophys. **176**(8), 3377–3390 (2019)
2. P. Akishin, M. Altaisky, I. Antoniou, A. Budnik, V. Ivanov, Burridge-knopoff model and self-similarity. Chaos, Solitons & Fractals **11**(1–3), 207–222 (2000)
3. C.H. Scholz, Earthquakes and friction laws. Nature **391**(6662), 37–42 (1998)
4. C.F. Richter, An instrumental earthquake magnitude scale. Bull. Seismol. Soc. Am. **25**(1), 1–32 (1935)
5. W.W. Doyel, A. Moraga B, E. Falcon M, Relation between the geology of valdivia, chile, and the damage produced by the earthquake of 22 May 1960. Bull. Seismol. Soc. Am. **53**(6), 1331–1345 (1963)
6. F. Lorenzo-Martín, F. Roth, R. Wang, Inversion for rheological parameters from post-seismic surface deformation associated with the 1960 valdivia earthquake, chile. Geophys. J. Int. **164**(1), 75–87 (2006)

7. A. Pomonis, The great chile earthquake sequence of may 21–22, 1960: an analysis of the human casualties by event, location and cause. Rep. Tono Res. Inst. Earthq. Sci. **28**, 17–20 (2011)
8. R. Burridge, L. Knopoff, Model and theoretical seismicity. Bull. Seismol. Soc. Am. **57**(3), 341–371 (1967)
9. G.L. Vasconcelos, First-order phase transition in a model for earthquakes. Phys. Rev. lett. **76**(25), 4865 (1996)
10. R. Montagne, G.L. Vasconcelos, Complex dynamics in a one-block model for earthquakes. Phys. A: Stat. Mech. Appl. **342**(1–2), 178–185 (2004)
11. B. Erickson, B. Birnir, D. Lavallée, A model for aperiodicity in earthquakes. Nonlinear Proc. Geophys. **15**(1), 1–12 (2008)
12. C. Marone, Laboratory-derived friction laws and their application to seismic faulting. Annu. Rev. Earth Planet. Sci. **26**(1), 643–696 (1998)
13. T.N. Nkomom, F.I. Ndzana, J.B. Okaly, A. Mvogo, Dynamics of nonlinear waves in a burridge and knopoff model for earthquake with long-range interactions, velocity-dependent and hydrodynamics friction forces. Chaos, Solitons & Fractals **150**, 111196 (2021)
14. T.N. Nkomom, J.B. Okaly, A. Mvogo, Dynamics of modulated waves and localized energy in a burridge and knopoff model of earthquake with velocity-dependant and hydrodynamics friction forces. Phys. A: Sta. Mech. Appl. **583**, 126283 (2021)
15. J.B. Okaly, A. Mvogo, R.L. Woulaché, T.C. Kofané, Nonlinear dynamics of damped dna systems with long-range interactions. Commun. Nonlinear Sci. Num. Simul. **55**, 183–193 (2018)
16. J. Okaly, A. Mvogo, C. Tabi, H. Ekobena Fouda, T. Kofané, Base pair opening in a damped helicoidal joyeux-buyukdagli model of dna in an external force field. Phys. Rev. E **102**(6), 062402 (2020)
17. J.B. Okaly, T. Nkoa Nkomom, Nonlinear dynamics of dna chain with long-range interactions. In: Nonlinear Dynamics of Nanobiophysics, pp. 67–96. Springer (2022)
18. V. Khain, M. Lomize, *Geotectonics with foundations of geodynamics* (Moscow State Univ, Moscow (in Russian), 1995)
19. H. Castaños, C. Lomnitz, Earthquake Disasters in Latin America: A Holistic Approach. Springer (2012)
20. K. Kasahara, Earthquake Mechanics vol. 248. Cambridge university press Cambridge (1981)
21. J. Carlson, J. Langer, Mechanical model of an earthquake fault. Phys. Rev. A **40**(11), 6470 (1989)
22. B.A. Erickson, B. Birnir, D. Lavallée, Periodicity, chaos and localization in a burridge-knopoff model of an earthquake with rate-and-state friction. Geophys. J. Int. **187**(1), 178–198 (2011)
23. S.A. Arsen'yev, L.V. Eppelbaum, T.B. Meirova, Discrete mathematical model of earthquake focus: An introduction. Pure Appl. Geophys. **177**(9), 4097–4118 (2020)
24. J.F. Bird, J.J. Bommer, Earthquake losses due to ground failure. Eng. Geol. **75**(2), 147–179 (2004)
25. D.K. Keefer, Landslides caused by earthquakes. Geol. Soc. Am. Bull. **95**(4), 406–421 (1984)
26. L. Lliboutry, La catastrophe du yungay (pérou). IAHS Publ. **104**, 353–363 (1975)
27. T. Gorum, C.J. Westen, O. Korup, M. Meijde, X. Fan, F.D. Meer, Complex rupture mechanism and topography control symmetry of mass-wasting pattern, 2010 haiti earthquake. Geomorphology **184**, 127–138 (2013)
28. D. Petley, S. Dunning, N. Rosser, A.B. Kausar, Incipient landslides in the jhelum valley, pakistan following the 8th october 2005 earthquake. Messages v (2006)
29. Y. Yin, F. Wang, P. Sun, Landslide hazards triggered by the 2008 wenchuan earthquake, sichuan, china. Landslides **6**(2), 139–152 (2009)
30. G. Domej, C. Bourdeau, L. Lenti, S. Martino, K. Pluta, Mean landslide geometries inferred from a global database of earthquake-and non-earthquake-triggered landslides. Ital. J. Eng. Geol. Environ. **2**(17), 87 (2017)
31. O. Norio, T. Ye, Y. Kajitani, P. Shi, H. Tatano, The 2011 eastern japan great earthquake disaster: Overview and comments. Int. J. Disaster Risk Sci. **2**(1), 34–42 (2011)
32. C. Xu, W. Sun, X. Zhou, Effects of huge earthquakes on earth rotation and the length of day. TAO: Terr., Atm. Ocean. Sci. **24**(4), 649 (2013)
33. T.-Q. Yun, Earthquake fastens earth rotation. Asian J. Geol. Res. **2**, 1–9 (2019)
34. C. Rodrıguez, J. Bommer, R. Chandler, Earthquake-induced landslides: 1980–1997. Soil Dyn. Earthq. Eng. **18**(5), 325–346 (1999)
35. F. Pelap, L. Kagho, C. Fogang, Chaotic behavior of earthquakes induced by a nonlinear magma up flow. Chaos, Solitons & Fractals **87**, 71–83 (2016)
36. P. Praveen Kumar, S. Balakrishnan, A. Magesh, P. Tamizharasi, Abdelsalam, S.I.: Numerical treatment of entropy generation and bejan number into an electroosmotically-driven flow of sutterby nanofluid in an asymmetric microchannel. Numerical Heat Transfer, Part B: Fundamentals, 1–20 (2024)
37. J.B. Okaly, A. Mvogo, R.L. Woulaché, T.C. Kofané, Semi-discrete breather in a helicoidal dna double chain-model. Wave Mot. **82**, 1–15 (2018)
38. M. Remoissenet, Low-amplitude breather and envelope solitons in quasi-one-dimensional physical models. Phys. Rev. B **33**(4), 2386 (1986)
39. T. Dauxois, M. Peyrard, Physics of Solitons. Cambridge University Press (2006)
40. R. Conte, M. Musette, Linearity inside nonlinearity: exact solutions to the complex ginzburg-landau equation. Phys. D: Nonlinear Phenom. **69**(1), 1–17 (1993). https://doi.org/10.1016/0167-2789(93)90177-3
41. V. Ginzburg, L. Landau, K teorii sverkhrovodimosti. Zhurnal Eksperimentalnoi i Teoreticheskoi Fiziki **20**, 1064–1082 (1950)
42. L.D. Landau, On the theory of phase transitions. i. Zh. Eksp. Teor. Fiz. 11, 19 (1937)
43. N. Akhmediev, A. Ankiewicz, Dissipative Solitons: from Optics to Biology and Medicine vol. 751. Springer, ??? (2008)
44. J.B. Okaly, F.I. Ndzana, R.L. Woulaché, C.B. Tabi, T.C. Kofané, Base pairs opening and bubble transport in damped dna dynamics with transport memory effects. Chaos: An Interdisciplinary Journal of Nonlinear Science 29(9), 093103 (2019)
45. I.S. Aranson, L. Kramer, The world of the complex ginzburg-landau equation. Rev. Mod. Phys. **74**(1), 99 (2002)
46. I. Carusotto, C. Ciuti, Quantum fluids of light. Rev. Mod. Phys. **85**(1), 299 (2013)
47. J.B. Okaly, F.I. Ndzana, R.L. Woulaché, T.C. Kofané, Solitary wavelike solutions in nonlinear dynamics of damped dna systems. Eur. Phys. J. Plus **134**(12), 598 (2019)